Sea Ice Changes in the Southwest Pacific Sector of the Southern Ocean During the Last 140,000 Years

Jacob Jones[1], Karen E Kohfeld[1,2], Helen Bostock[3,4], Xavier Crosta[5], Melanie Liston[6], Gavin Dunbar[6], Zanna Chase[7], Amy Leventer[8] Harris Anderson[7], Geraldine Jacobsen[9]

[1] School of Resource and Environmental Management, Simon Fraser University, Burnaby, Canada
[2] School of Environmental Science, Simon Fraser University, Burnaby, Canada
[3] School of Earth and Environmental Sciences, The University of Queensland, Brisbane, Australia
[4] National Institute of Water and Atmospheric Research (NIWA), Wellington, New Zealand
[5] Université de Bordeaux, CNRS, EPHE, UMR 5805 EPOC, Pessac, France
[6] Antarctic Research Centre, Victoria University of Wellington, Wellington, New Zealand
[7] Institute of Marine and Antarctic Studies, University of Tasmania, Hobart, Australia
[8] Geology Department, Colgate University, Hamilton, NY, USA
[9] Centre for Accelerator Science, Australian Nuclear Science and Technology Organisation, Lucas Heights, NSW, Australia

Correspondence to: Jacob Jones (jacob_jones@sfu.ca)

Abstract

Sea ice expansion in the Southern Ocean is believed to have contributed to glacial-interglacial atmospheric CO_2 variability by inhibiting air-sea gas exchange and influencing the ocean's meridional overturning circulation. However, limited data on past sea ice coverage over the last 140 ka (a complete glacial cycle) have hindered our ability to link sea ice expansion to oceanic processes that affect atmospheric CO_2 concentration. Assessments of past sea ice coverage using diatom assemblages have primarily focused on the Last Glacial Maximum (~21 ka BP) to Holocene, with few quantitative reconstructions extending to the onset of glacial Termination II (~135 ka BP). Here we provide new estimates of winter sea ice concentrations (WSIC) and summer sea surface temperatures (SSST) for a full glacial-interglacial cycle from the southwestern Pacific sector of the Southern Ocean using the Modern Analog Technique (MAT) on fossil diatom assemblages from deep-sea core TAN1302-96. We examine how the timing of changes in sea ice coverage relates to ocean circulation changes and previously proposed mechanisms of early glacial CO_2 drawdown. We then place SSST estimates within the context of regional SSST records to better understand how these surface temperature changes may be influencing oceanic CO_2 uptake. We find that winter sea ice was absent over the core site during the early glacial period until MIS 4 (~65 ka BP), suggesting that sea ice may not have been a major contributor to early glacial CO_2 drawdown. Sea ice expansion throughout the glacial-interglacial cycle, however, appears to coincide with observed regional reductions in Antarctic Intermediate Water production and subduction, suggesting that sea ice may have influenced intermediate ocean circulation changes. We observe an early glacial (MIS 5d) weakening of meridional SST gradients between 42˚ to 59˚S throughout the region, which may have contributed to early reductions in atmospheric CO_2 concentrations through its impact on air-sea gas exchange.

42

1.0 Introduction

43

44   Antarctic sea ice has been suggested to have played a key role in glacial-interglacial

45 atmospheric CO_2 variability (e.g., Stephens & Keeling, 2000; Ferrari et al., 2014; Kohfeld &

46 Chase, 2017; Stein et al., 2020). Sea ice has been dynamically linked to several processes that

47 promote deep ocean carbon sequestration, namely by: [1] reducing deep ocean outgassing by

48 ice-induced 'capping' and surface water stratification (Stephens & Keeling, 2000; Rutgers van

49 der Loeff et al., 2014), and [2] influencing ocean circulation through water mass formation and

50 deep-sea stratification, leading to reduced diapycnal mixing and reduced CO_2 exchange

51 between the surface and deep ocean (Toggweiler, 1999; Bouttes et al., 2010; Ferrari et al.,

52 2014). Numerical modelling studies have shown that sea ice-induced capping, stratification, and

53 reduced vertical mixing may be able to account for a significant portion of the total CO_2

54 variability on glacial-interglacial timescales (between 40-80 ppm) (Stephens & Keeling, 2000;

55 Galbraith & de Lavergne, 2018; Marzocchi & Jansen, 2019; Stein et al., 2020). However, debate

56 continues surrounding the timing and magnitude of sea ice impacts on glacial-scale carbon

57 sequestration (e.g., Morales Maquede & Rahmstorf, 2002; Archer et al., 2003; Sun &

58 Matsumoto, 2010; Kohfeld & Chase, 2017).

59   Past Antarctic sea ice coverage has been estimated primarily through diatom-based

60 reconstructions, with most work focusing on the Last Glacial Maximum (LGM), specifically the

61 EPILOG timeslice as outlined in Mix et al. (2001), corresponding to 23 to 19 thousand years ago

62 (ka) before present (BP). During the LGM, these reconstructions suggest that winter sea ice

63 expanded by 7-10° latitude (depending on the sector of the Southern Ocean), which

64 corresponds to substantial expansion of total winter sea ice coverage compared to modern

65 observations (Gersonde et al., 2005; Benz et al., 2016; Lhardy et al., 2021). Currently, only a

66 handful of studies provide quantitative sea-ice coverage estimates back to the penultimate

67 glaciation, Marine Isotope Stage (MIS) 6 (~194 to 135 ka BP) (Gersonde & Zielinksi, 2000; Crosta

68 et al., 2004; Schneider-Mor et al., 2012; Esper & Gersonde 2014a; Ghadi et al. 2020). These

69 studies primarily cover the Atlantic sector, with only one published sea ice record from each of

70 the Indian (SK200-33 from Ghadi et al., 2020), eastern Pacific (PS58/271-1 from Esper &

71 Gersonde, 2014a), and southwestern Pacific sectors (SO136-111 from Crosta et al., 2004).

72 These glacial-interglacial sea ice records show heterogeneity between sectors in both timing

73 and coverage. While the Antarctic Zone (AZ) in the Atlantic sector experienced early sea ice

74 advance corresponding to MIS 5d cooling (i.e., 115 to 105 ka BP) (Gersonde & Zielinksi, 2000;

75 Bianchi & Gersonde, 2002; Esper & Gersonde, 2014a), the Indian and Pacific sector cores in the

76 AZ show only minor sea ice advances during this time (Crosta et al., 2004; Ghadi et al., 2020).

77 The lack of spatial and temporal resolution has resulted in significant uncertainty in our ability

78 to evaluate the timing and magnitude of sea ice change during a full glacial cycle across the

79 Southern Ocean, and to link sea ice to glacial-interglacial CO_2 variability.

80   This paper provides new winter sea ice concentration (WSIC) and summer sea surface

81 temperature (SSST) estimates for the southwestern Pacific sector of the Southern Ocean over

82 the last 140 ka BP. WSIC, which is a grid-scale observation of the mean state fraction of ocean

83 area that is covered by sea ice over the sample period, and SSST estimates are produced by

84 applying the Modern Analog Technique (MAT) to fossil diatom assemblages from sediment core

85 TAN1302-96 (59.09°S, 157.05°E, water depth 3099 m). We place this record within the context

86 of sea ice and SSST changes from the region using previously published records from SO136-111

87 (56.66°S, 160.23°E, water depth 3912 m), which has recalculated WSIC and SSST estimates

88 presented in this study, and nearby marine core E27-23 (59.61°S, 155.23°E; water depth 3182

89 m) (Ferry et al., 2015). Using these records, we compare the timing of sea ice expansion to early

90 glacial-interglacial CO_2 variability to test the hypothesis that the initial CO_2 drawdown (~115 to

91 100 ka BP) resulted from reduced air-sea gas exchange in response to sea ice capping and

92 surface water stratification (Kohfeld and Chase, 2017). We then consider alternative oceanic

93 drivers of early atmospheric CO_2 variability and place our SSST estimates within the context of

94 other studies to examine how regional cooling and a weakening in meridional SST gradients

95 might affect air-sea disequilibrium and early CO_2 drawdown (Khatiwala et al., 2019). Finally, we

96 compare our WSIC estimates with regional reconstructions of Antarctic Intermediate Water

97 (AAIW) production and subduction variability using previously published carbon isotope

98 analyses on benthic foraminifera from intermediate to deep-water depths in the southwest

99   Pacific sector of the Southern Ocean, to test the hypothesis that sea ice expansion is

100   dynamically linked to AAIW production and variability (Ronge et al., 2015).

101

2.0 Methods

2.1 Study Site and Age Determination

104   We reconstruct diatom-based WSIC and SSST using marine sediment core TAN1302-96

105   (59.09°S, 157.05°E, water depth 3099 m) (Figure 1). The 364 cm core was collected in March

106   2013 using a gravity corer during the return of the *RV Tangaroa* from the Mertz Polynya in

107   Eastern Antarctica (Williams et al., 2013). The core is situated in the western Pacific sector of

108   the Southern Ocean, on the southwestern side of the Macquarie Ridge, approximately 3-4°

109   south of the average position of the Polar Front (PF) at 157°E (Sokolov & Rintoul, 2009).

110
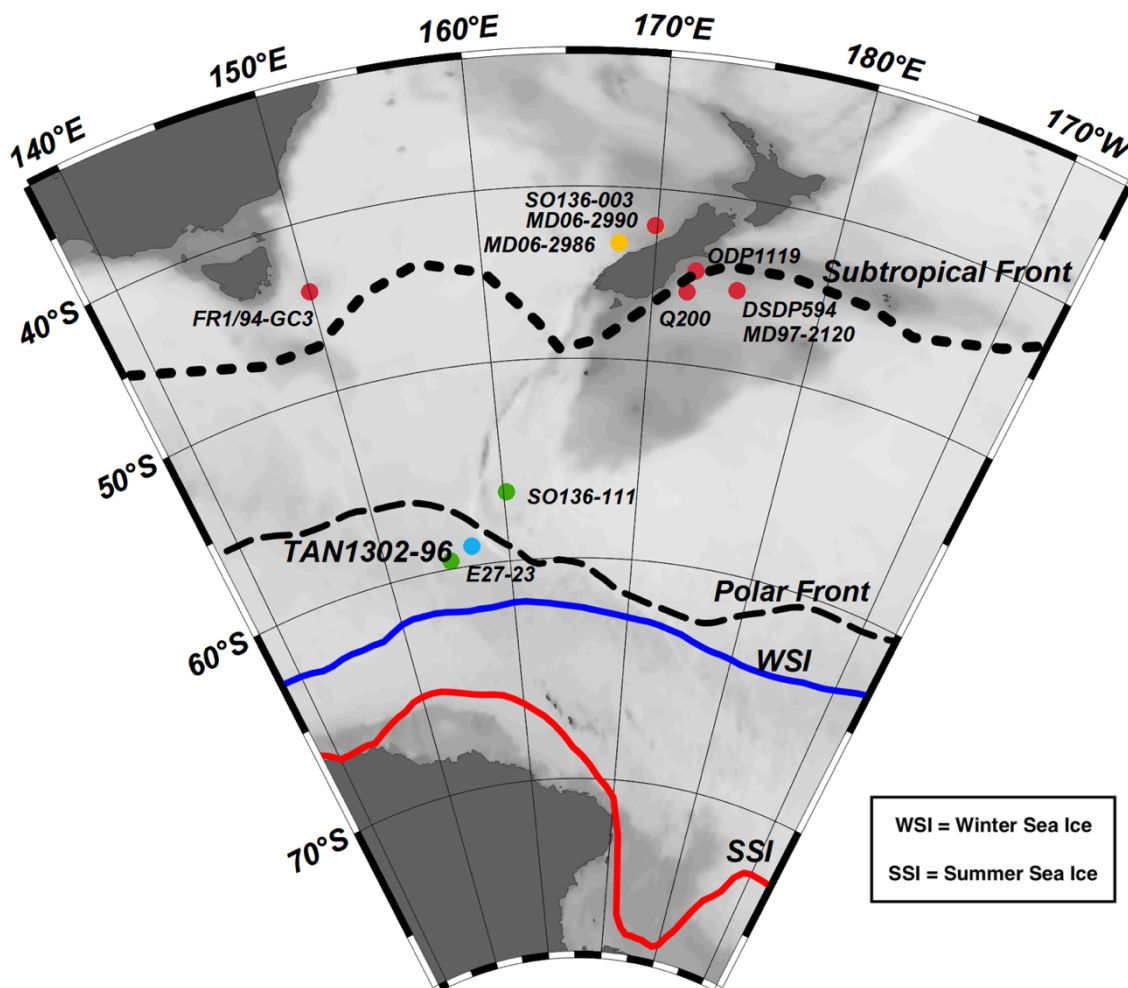
Figure 1: Map of the southwestern Pacific sector of the Southern Ocean including the study site, TAN1302-96 (blue circle), and additional published cores providing sea ice extent data, SO136-111 and E27-23 (green circles), SST reconstructions (red circles), and δ^{13}C of benthic foraminifera (yellow circles). Note that some cores may not appear present in the figure because of their proximity to other cores. Data for all cores are provided in Table 2. Dashed lines show the average location of the Subtropical and Polar Fronts (Smith et al., 2013; Bostock et al., 2015), and red and blue lines show mean positions of modern summer sea ice (SSI) and winter sea ice (WSI) extents, respectively (Reynolds et al., 2002; 2007).

The age model for TAN1302-96 (Figures 2 and 3) was based on a combination of radiocarbon dating of mixed foraminiferal assemblages and stable oxygen isotope stratigraphy on *Neogloboquadrina pachyderma* (180-250 μm). Seven accelerator mass spectrometry (AMS) ^{14}C samples were collected (Table A1 in Appendix A) and consisted of mixed assemblages of planktonic foraminifera (*N. pachyderma* and *Globigerina bulloides,* >250 μm). Three of the seven radiocarbon samples (NZA 57105, 57109, and 61429) were previously published in Prebble et al. (2017), and four additional samples (OZX 517-520) were added to improve the dating reliability (Table A1 in Appendix A). OZX 519 and OZX 520 produced dates that were not distinguishable from background (>57.5 ka BP) and were subsequently excluded from the age model. The TAN1302-96 oxygen isotopes were run at the National Institute of Water and Atmospheric Research (NIWA) using the Kiel IV individual acid-on-sample device and analysed using Finnigan MAT 252 Mass Spectrometer. The precision is ±0.07% for δ^{18}O and ±0.05% for δ^{13}C.

The age model was constructed using the 'Undatable' MATLAB software by bootstrapping at 10% and using an x-factor of 0.1 (Lougheed & Obrochta, 2019), which scales Gaussian distributions of sediment accumulation uncertainty (Table A2 in Appendix A). Below 100 cm, 9 tie points were selected at positions of maximum change in δ^{18}O and were correlated to the LR04 benthic stack (Lisiecki & Raymo, 2005) (Fig 2; Table A2 in Appendix A). Uncertainty associated with stratigraphic correlation to the LR04 stack has been estimated to be ± 4 ka (Lisiecki & Raymo, 2005). We used a conservative marine reservoir age (MRA) for radiocarbon calibration of 1000 +/- 100 years, in line with regional estimates in Paterne et al. (2019) and modelled estimates by Butzin et al. (2017; 2020). The age model shows that TAN1302-96

142   extends to at least 140 ka BP, capturing a full glacial-interglacial cycle. Linear sedimentation

143   rates (LSR) in TAN1302-96 were observed to be higher during interglacial periods, averaging

144   ~3.5 cm ka⁻¹, compared to glacial periods, averaging ~2.5 cm ka⁻¹. It is worth noting that there

145   can be significant MRA variability over time due changes in ocean ventilation, sea ice coverage,

146   and wind strength, specifically in the polar high latitudes (Heaton et al., 2020), and as a result,

147   caution should be taken when interpreting the precision of radiocarbon dates. For more

148   information on age model construction and selection, refer to the supplemental online

149   materials (SOM).

150
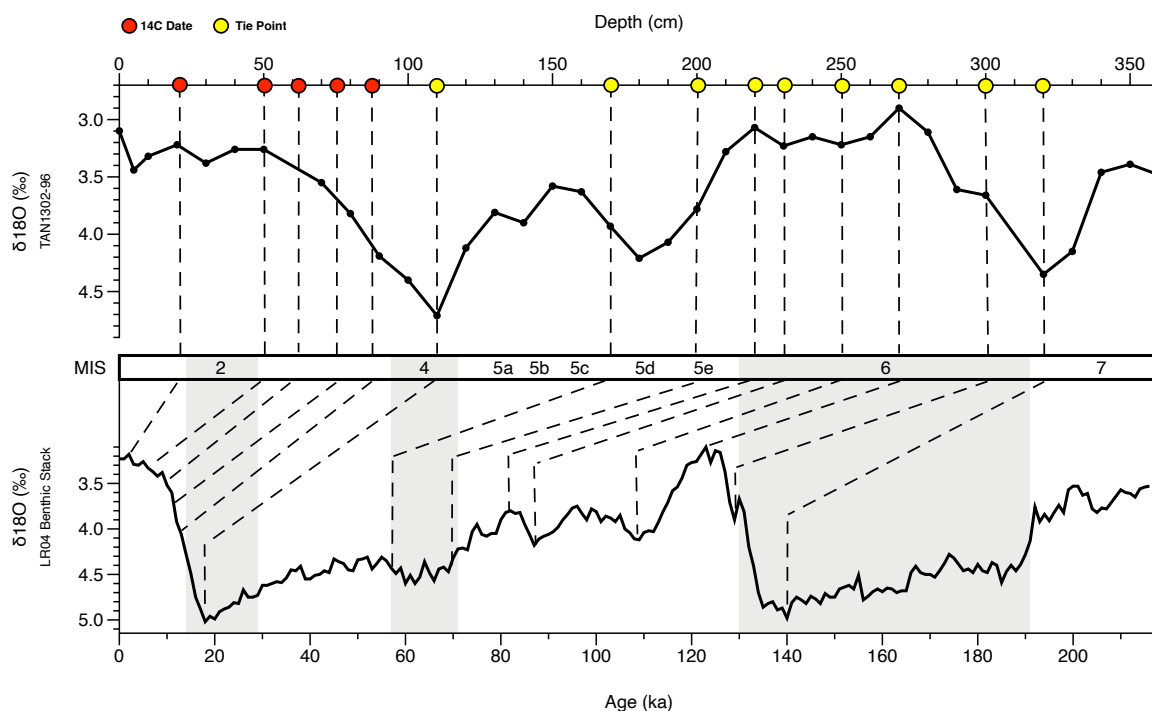
151   **Figure 2:** Age model of TAN1302-96. Red circles indicate the depth of AMS ¹⁴C samples and
152   yellow circles indicate tie points between the TAN1302-96 oxygen isotope stratigraphy and the
153   LR04 benthic stack (Lisiecki & Raymo, 2005). Two radiocarbon dates, OZX 519 & 520 (at 130 and
154   170 cm, respectively), were not included in the age model as they produced dates that were
155   NDFB (not distinguishable from background).

156
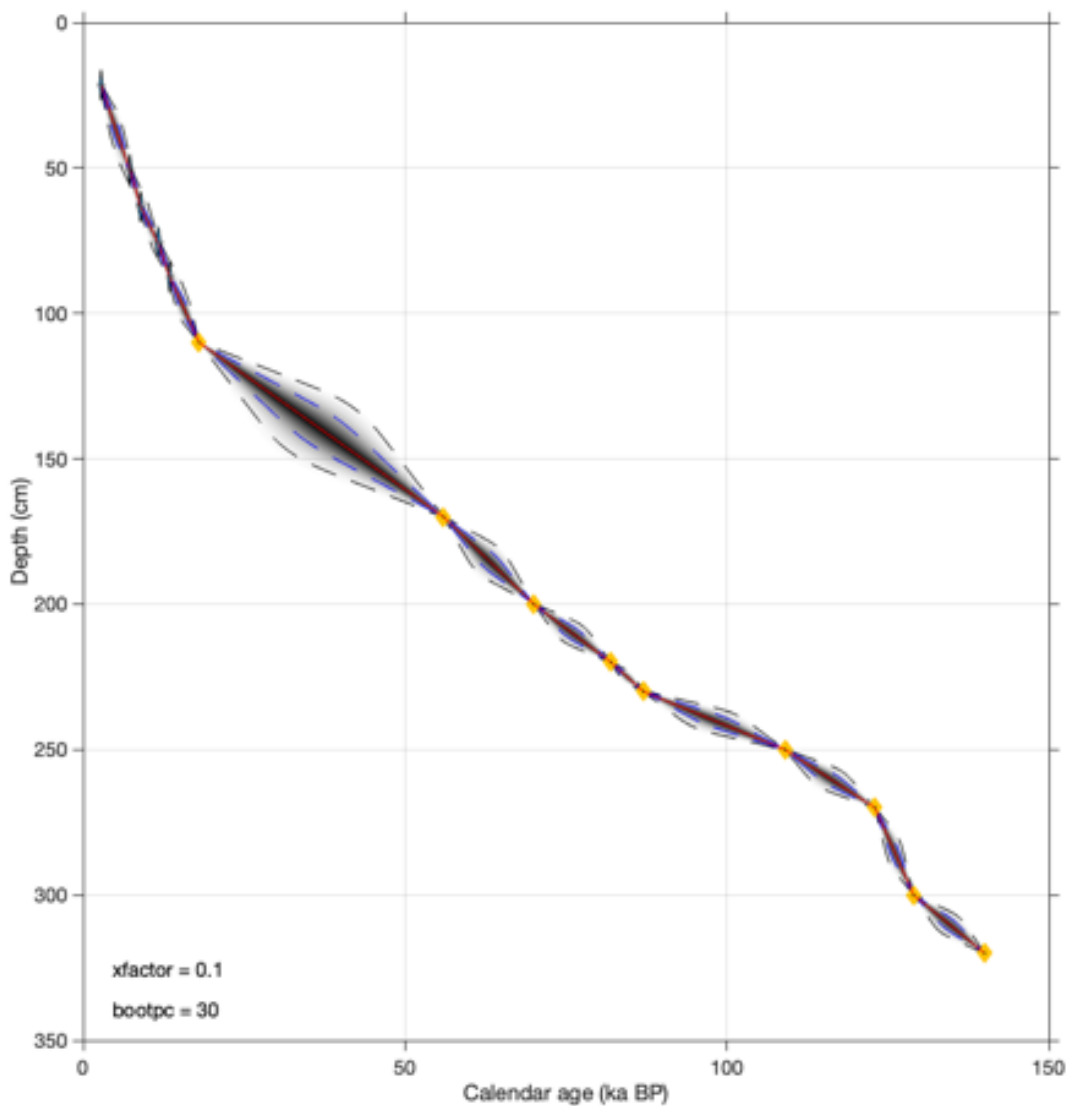
Figure 3: Age model of TAN1302-96. Tie points are depicted as yellow dots and grey shading represents associated uncertainty between tie points. The age model used a marine reservoir calibration of 1000 +/- 100 years.

2.2 Diatom Analysis

TAN1302-96 was sampled every 3-4 cm throughout the core except between 130-180

cm, where samples were collected every 10 cm due to limited availability of sample materials

(Table A3 in Appendix A). Diatom slide preparation followed two procedures. The first approach

165 approximated the methods outlined in Renberg (1990), while the second followed the protocol

166 outlined in Warnock & Scherer (2015). To ensure there were no biases between preparation

167 techniques, results from each technique were first visually compared followed by a comparison

168 of sample means (see Figure B1 in Appendix B). No biases in the data were observed between

169 methods.

170   The first procedure was conducted at Victoria University of Wellington and Simon Fraser

171 University on samples every 10 cm throughout the core. Sediment samples contained high

172 concentrations of diatoms with little carbonaceous or terrigenous materials, so no dissolving

173 aids were used. Instead, approximately 50 mg of sediment was weighed, placed into a 50 ml

174 centrifuge tube, and topped up with 40 ml of deionized water. Samples were then manually

175 shaken to disaggregate sediment, followed by a 10-second mechanical stir using a vortex

176 machine. Samples were then left to settle for 25 seconds. 0.25 mL of the solution was then

177 pipetted onto a microscope slide from a consistent depth, where it was left to dry overnight.

178 Once the sample had dried, coverslips were permanently mounted to the slide using Permount,

179 a high refractive index mountant. Slides were redone if they contained too many diatoms and

180 identification was not possible, or if they contained too few diatoms (generally <40 specimens

181 per transect). Sediment sample weight was adjusted to achieve the desired dilution.

182   The second procedure was conducted at Colgate University on samples every 3-4 cm

183 throughout the core. Oven-dried samples were placed into a 20 ml vial with 1-2 ml of 10% H_2O_2

184 and left to react for up to several days, followed by a brief (2-3 second) ultrasonic bath to

185 disaggregate samples. The diatom solution was then added into a settling chamber, where

186 microscope coverslips were placed on stages to collect settling diatoms. The chamber was

187 gradually emptied through an attached spigot, and samples were evaporated overnight. Cover

188 slips were permanently mounted onto the slides with Norland Optical Adhesive #61, a

189 mounting medium with a high refractive index.

190   Diatom identification was conducted at Simon Fraser University using a Leica Leitz

191 DMBRE light microscope using standard microscopy techniques. Following transverses, a

192 minimum of 300 individual diatoms were identified at 1000x magnification from each sample

193 throughout the core. Individuals were counted towards the total only if they represented at

194   least one-half of the specimen so that fragmented diatoms were not counted twice.

195   Identification was conducted to the highest taxonomic level possible, either to the species or

196   species-group level. Taxonomic identification was conducted using numerous identification

197   materials, including (but not limited to): Fenner et al. (1976); Fryxell & Hasle (1976; 1980);

198   Johansen & Fryxell (1985); Hasle & Syversten (1997); Cefarelli et al. (2010); and Wilks & Armand

199   (2017). The relative abundances were calculated by dividing the number of identified

200   specimens of a particular species by the total number of identified diatoms from the sample.

201   Based on previously established taxonomic groups (Crosta et al., 2004), diatoms were grouped

202   into one of three categories based on temperature preference and sea ice tolerance. The

203   following main taxonomic groups were used (Table 1):

204

205   **[1]** Sea Ice Group: representing diatoms that thrive in or near the sea ice margin in SSTs

206   generally ranging from -1 to 1 °C.

207   **[2]** Permanent Open Ocean Zone (POOZ): representing diatoms that thrive in open

208   ocean conditions, with SSTs generally ranging from ~2 to 10 °C.

209   **[3]** Sub-Antarctic Zone (SAZ): representing diatoms that thrive in warmer sub-Antarctic

210   waters, with SSTs generally ranging from 11 to 14 °C.

211

212   **Table 1**: Species comprising each of the diatom taxonomic groups (updated from Crosta et al.,
213   2004).

Sea Ice Group	POOZ Group	SAZ Group
Actinocyclus actinochilus	*Fragilariopsis kerguelensis*	*Azpeitia tabularis*
Fragilariopsis curta	*Fragilariopsis rhombica*	*Hemidiscus cuneiformis*
Fragilariopsis cylindrus	*Fragilariopsis separanda*	*Thalassionema nitzschioides var. lanceolata*
Fragilariopsis obliquecostata	*Rhizosolenia polydactyla* var. *polydactyla*	*Thalassiosira eccentrica*
Fragilariopsis ritscheri	*Thalassionema nitzschioides* (form 1)	*Thalassiosira oestrupii* gp.
Fragilariopsis sublinearis	*Thalassiosira gracilis* gp.	
	Thalassiosira lentiginosa	
	Thalassiosira oliverana	
	Thalassiothrix sp.	
	Trichotoxon reinboldii	

214

2.3 Modern Analog Technique

Past WSIC and SSST (January to March) were estimated for TAN1302-96 and recalculated for SO136-111 by applying the Modern Analog Technique (MAT) to the fossil diatom assemblages, as outlined in Crosta et al. (1998; 2020). Summer (January to March) SST was estimated because it is considered to be a better explanatory variable than spring or annual SST (Esper et al., 2010; Esper & Gersonde, 2014b). The MAT reference database used for this analysis is comprised of 249 modern core top samples (analogs) located primarily in the Atlantic and Indian sectors from ~40°S to the Antarctic coast. The age of the core tops included in the reference database have been assessed through radiocarbon and/or isotope stratigraphy when possible. Core tops were visually evaluated for selective diatom dissolution, so it is believed that sub-modern assemblages contain well-preserved and unbiased specimens. Modern SSST and WSIC were interpolated from the reference core locations using a 1°x1° grid from the World Ocean Atlas (Locarnini et al., 2013) through the Ocean Data View (Schlitzer, 2005). The MAT was applied using the "bioindic" package (Guiot & de Vernal, 2011) through the R-platform. Fossil diatom assemblages were compared to the modern analogs using 33 species or species-groups to identify the five most similar modern analogs using both the LOG and CHORD distance. The dissimilarity threshold, above which the fossil assemblages are considered to be too dissimilar to the modern dataset, is fixed at the first quartile of random distances (Crosta et al., 2020). The reconstructed SSST and WSIC are the distance-weighted mean of the climate values associated with the selected modern analog (Guiot et al., 1993; Ghadi et al., 2020). Both MAT approaches produce an R^2 value of 0.96 and a root mean square error of prediction (RMSEP) of ~1°C for SSST, and an R^2 of 0.93 and a RMSEP of 10% for WSIC (Ghadi et al. 2020). As outlined in Ferry et al., (2015), we consider <15% WSIC to represent an absence of winter sea ice, 15-40% WSIC as present but unconsolidated, and >40% to represent consolidated winter sea ice.

2.4 Additional Core Data

We use additional published marine cores from the southwestern Pacific throughout this analysis (Table 2), for WSIC comparisons (E27-23), %AAIW calculations (MD06-2990/SO136-

244   003, MD06-2986, and MD97-2120), and regional SST gradient comparisons (SO136-003,

245   FR1/94-GC3, ODP 1119-181, DSDP 594, and Q200).

246   **Table 2**: Additional data on published marine cores used throughout this analysis.

Core Name	Latitude	Longitude	Depth	Age Model Reference	Data Assessed	Data Source
TAN1302-96	59.09°S	157.05°E	3099 m	*This study*	WSIC; SST	*This study*
SO136-111	56.66°S	160.23°E	3912 m	Crosta et al. (2004)	WSIC; SST	Crosta et al. (2004); *recalculated in this study*
E27-23	57.65°S	155.23°E	3182 m	Ferry et al. (2015)	WSIC	Ferry et al. (2015)
MD06-2990	42.01°S	169.92°E	943 m	Ronge et al. (2015)	δ13C	Ronge et al. (2015)
MD06-2986	43.45°S	167.9°E	1477 m	Ronge et al. (2015)	δ13C	Ronge et al. (2015)
MD97-2120	45.54°S	174.94°E	121 0m	Pahnke & Zahn (2005)	δ13C	Pahnke & Zahn (2005)
SO136-003	42.3°S	169.88°E	958 m	Pelejero et al. (2006); Barrows et al. (2007)	δ13C; SST	Pelejero et al. (2006); Ronge et al. (2015)
FR1/94-GC3	44.25°S	149.98°E	2667 m	Pelejero et al. (2006)	SST	Pelejero et al. (2006)
ODP 1119-181	44.75°S	172.39°E	396 m	Wilson et al. (2005)	SST	Wilson et al. (2005); Hayward et al. (2008)
DSDP 594	45.54°S	174.94°E	1204 m	Nelson et al. (1985); Kowalski & Meyers (1997)	SST	Schaefer et al. (2005)
Q200	45.99°S	172.02°E	1370 m	Waver et al., 1998	SST	Weaver et al. (1998)

247

3.0 Results

3.1 TAN1302-96 Diatom Assemblage Results

250   In this core, fifty-one different species or species groups were identified, of which 33

251   were used in the transfer function. These 33 species represent >82% of the total diatom

252   assemblages (mean of 92%). Permanent Open Ocean Zone (POOZ) diatoms made up the largest

253   proportion of diatoms identified, representing between 72-91% of the assemblage (Figure 4),

254   with higher values observed during warmer interstadial periods of MIS 1, 3, and 5. Sea ice

255   diatoms made up the second most abundant group, representing between 0.5-7.5% of the

256   assemblage, with higher values observed during cooler stadial periods (MIS 2, 4, and 6). The

257   Sub-Antarctic Zone group had relatively low abundances, with higher values occurring during

258   warmer interstadial periods (MIS 5 and the Holocene) and briefly during MIS 4 at ~65 ka BP.

259
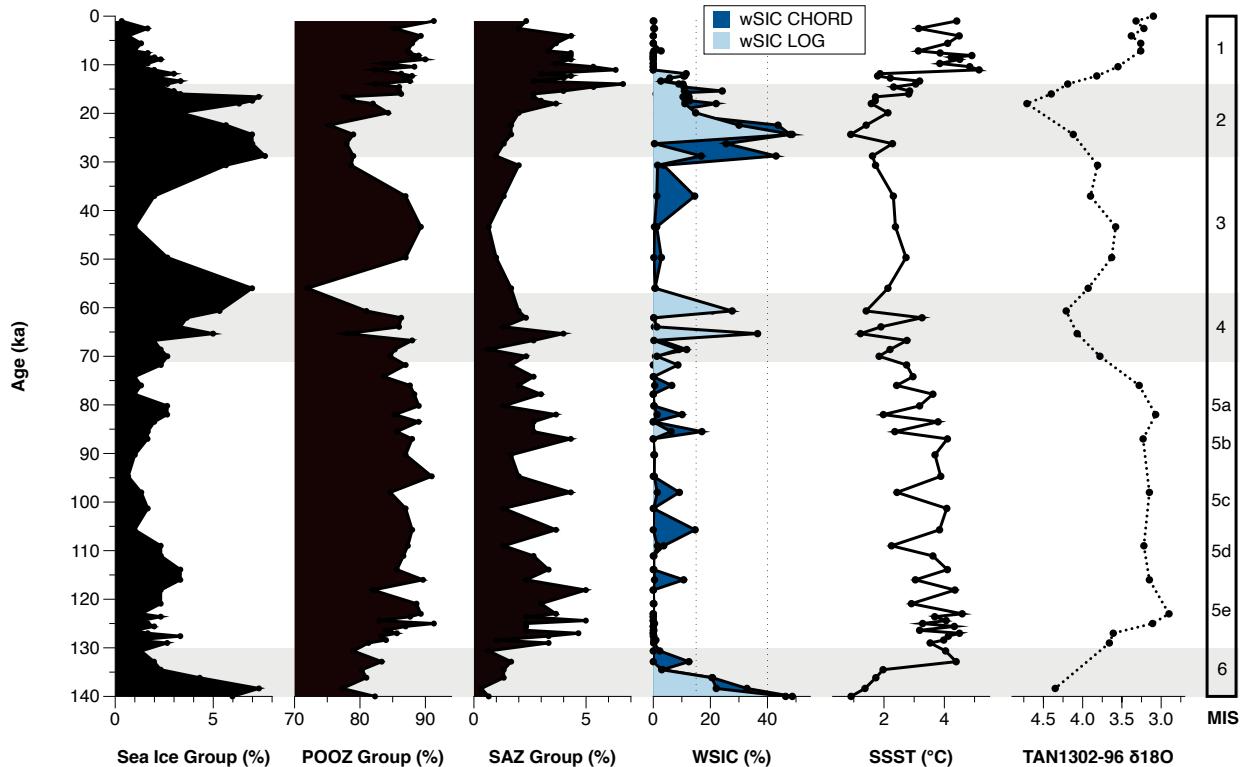
Figure 4: Diatom assemblages results from TAN1302-96 separated into % contribution from each taxonomic group (Sea ice Group, POOZ, and SAZ; see Table 1) over a full glacial-interglacial cycle. Using the Modern Analog Technique (MAT), winter sea ice concentration (WSIC) and summer sea surface temperature (SSST) were estimated and compared against the $\delta^{18}O$ signature of TAN1302-96.

3.2 TAN1302-96 SSST and WSIC Estimates

There were no non-analog conditions observed in TAN1302-96 samples and all estimates were calculated on five analogs. Estimates of SSST and WSIC from both LOG and CHORD MAT outputs produced similar results (Figure 4). During Termination II, SSST began to rise from ~1°C at 140 ka BP (MIS 6) to ~4.5°C at 132 ka BP (MIS 5e/6 boundary). This warming corresponded with a decrease in WSIC from 48% to approximately 0% over the same time periods (Figure 4). Reconstructed SSST were variable throughout MIS 5e, reaching a maximum value of ~4.5°C at 118 ka BP, after which they declined throughout MIS 5. During this period of SSST decline, winter sea ice was largely absent, punctuated by brief periods during which sea ice was present but unconsolidated (WSIC = ~15% and 17% at 105 and 85 ka BP, respectively). During MIS 4 (71 to 57 ka BP), SSST cooled to between roughly 1°C and 3°C, and sea ice

277   expanded to 36%, such that it was present but unconsolidated for intervals of a few thousand

278   years. SSST increased slightly from 1.5°C at 61 ka BP (during MIS 4) to ~2.5°C at 50 ka BP (during

279   MIS 3), followed by a general cooling trend into MIS 2. Sea ice appears to have been largely

280   absent during MIS 3 (57 to 29 ka BP), although sampling resolution is low, but increased rapidly

281   to 48% cover during MIS 2 where winter sea ice was consolidated over the core site. During MIS

282   2, SSST cooled to a minimum of <1°C at 24.5 ka BP. After 18 ka BP, the site rapidly transitioned

283   from cool, ice-covered conditions to warmer, ice-free winter conditions during the early

284   deglaciation. This warming was interrupted by a brief cooling around 13.5 ka BP, following

285   which SSST quickly reached their maximum values of ~5°C at 11.5 ka BP and remained relatively

286   high throughout the rest of the Holocene. Winter sea ice was not present during the Holocene.

287

288   **3.3 SO136-111 SSST and WSIC Recalculation**

289   In core SO136-111, the 33 species included in the transfer function represent values

290   >79% of the total diatom assemblages (mean of 91%). There were no non-analog conditions

291   observed in SO136-111 samples and all estimates were calculated on five analogs. Recalculated

292   estimates of SSST and WSIC from both LOG and CHORD MAT outputs produced similar results

293   for SO136-111 (Figure 5a, 5d). During Termination II, SSST rose from ~2°C at 137 ka BP (MIS 6)

294   to a maximum value of 6°C at 125 ka BP (MIS 5e), corresponding to a rapid decline in WSIC from

295   37% to ~0% during the same period. SSST remained relatively high (between 4 and 5°C) from

296   125 ka BP until 115 ka BP where they declined to ~2°C. SSST remained variable from 110 ka BP

297   until ~40 ka BP, fluctuating between ~2°C and 4°C. Winter sea ice was largely absent during MIS

298   5, with a brief period where sea ice was present but unconsolidated (WSIC = 17% at 84 ka).

299   Beginning at ~76 ka BP, WSIC began to increase and continued throughout early MIS 4 to a

300   maximum 36% at 69 ka BP. WSIC remained present but unconsolidated throughout most of MIS

301   3 and 2 with brief periods of absence (WSIC = <15%) lasting a few thousand years. SSST and

302   WSIC reached their coolest values and highest concentration at 24.5 ka before SSST increased

303   to ~5°C and stabilized throughout the Holocene, while WSIC declined to virtually 0% throughout

304   the same period.

305

4.0 Discussion

4.1 Regional SSST and WSIC Estimates

The new WSIC and SSST estimates from TAN1302-96 and recalculated WSIC estimates from SO136-111 show a coherent regional pattern (Figure 5). TAN1302-96 shows slightly higher concentrations during MIS 2 (max WSIC = 48% at 24.5 ka BP) and 4 (max WSIC = 37% at 65 ka BP) compared with SO136-111 (max WSIC = 35% at 24.5 ka BP and 36% at 68 ka BP, respectively), which can be explained by a more poleward position of TAN1302-96 relative to SO136-111. The estimates between cores differ during MIS 3, with seemingly lower WSIC in TAN1302-96 than in SO136-111, which might result from the low sampling resolution in TAN1302-96 during this period. Overall, these cores show a highly similar and coherent history of sea ice over the last 140 ka BP.
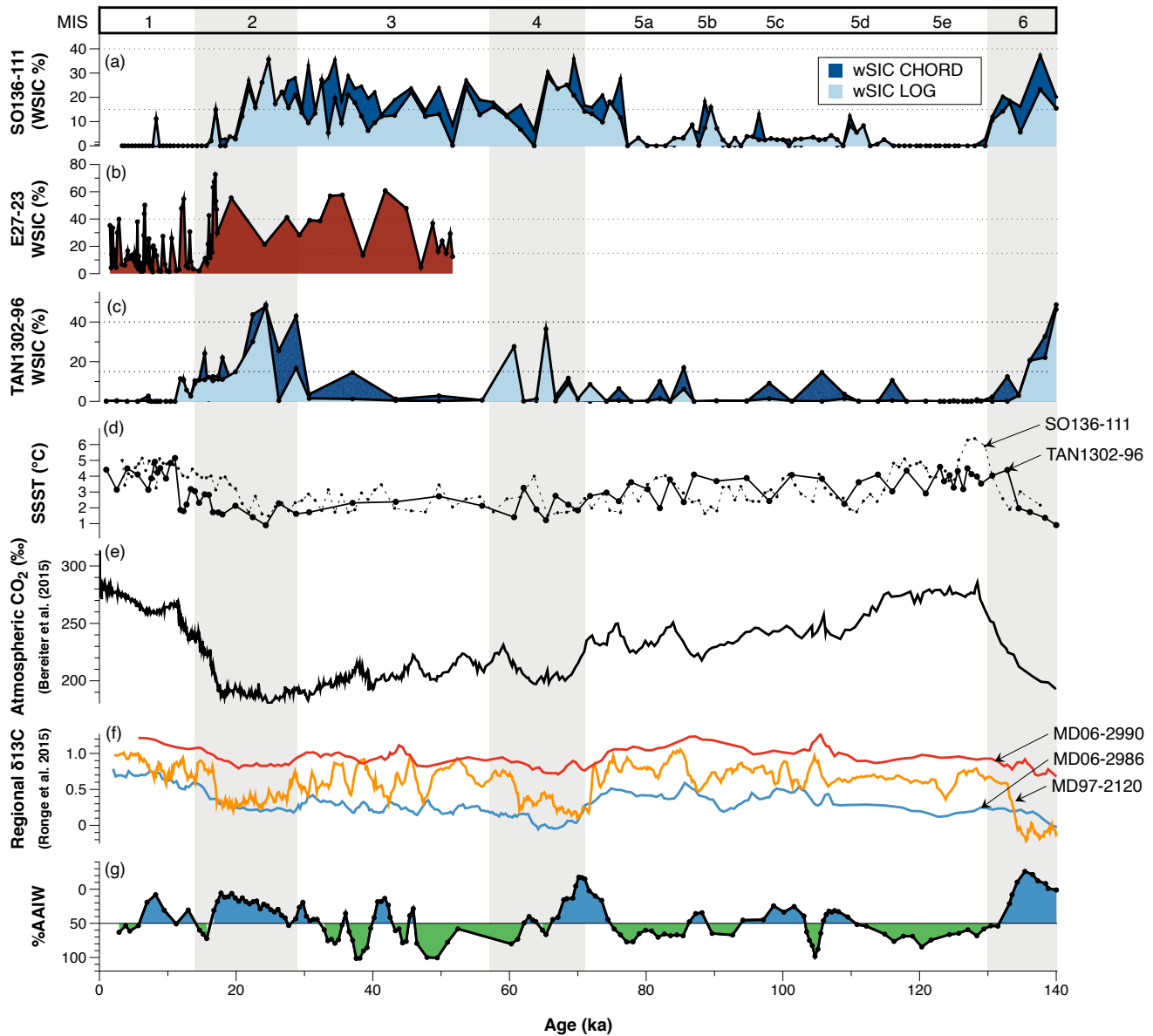
Figure 5: (a) WSIC estimates using MAT from SO136-111 (recalculated in this study, see
Appendix D); **(b)** WSIC estimates using GAM from E27-23 (Ferry et al., 2015); **(c)** WSIC estimates
using MAT from TAN1302-96 (this study); **(d)** SSST estimates using MAT from TAN1302-96 (solid
black line) and recalculated SSST for SO136-111 (black dotted line); **(e)** Antarctic atmospheric
CO_2 concentrations over 140 ka BP (Bereiter et al., 2015); **(f)** $\delta^{13}C$ data from nearby cores
MD06-2990/SO136-003, MD97-2120, and MD06-2986 (Ronge et al., 2015); **(g)** %Antarctic
Intermediate Water (%AAIW) as calculated in Ronge et al. (2015), which tracks when core
MD97-2120 was bathed primarily by AAIW (green) or Upper Circumpolar Deep Water (UCDW)
(blue).

328   When compared with E27-23 (Figure 5b), which is located only ~120 km to the

329   southwest of TAN1302-96 (Figure 1), the TAN1302-96 core shows lower estimates of WSIC,

330   especially during MIS 3. During early and mid-MIS 2, both cores show similar WSIC estimates,

331   while later in MIS 2 (~17 ka BP), E27-23 reports a maximum WSIC of 72% compared to only 22%

332   at TAN1302-96. A discrepancy between estimates is also observed during the Holocene, with

333   E27-23 reporting sea ice estimates of up to nearly 50% during the mid-Holocene (~6 ka BP),

334   while TAN1302-96 experienced values well below the RMSEP of 10%.

335   Possible explanations for the observed differences in WSIC estimates include: [1]

336   differences in statistical applications; [2] lateral sediment redistribution; [3] differences in

337   laboratory protocols; [4] differences in diatom identification/counting methodology; and [5]

338   selective diatom dissolution. Of these explanations, we believe that [1] and [2] are the most

339   likely candidates and are discussed below (for further discussion on [3], [4], and [5], see

340   Appendix C).

341   The first possible explanation is the use of different statistical applications. Ferry et al.

342   (2015) used a Generalized Additive Model (GAM) to estimate WSIC for both E27-23 and SO136-

343   111, while we have used the MAT for TAN1302-96 and SO136-111. A simple comparison of

344   WSIC estimates between the results in Ferry et al. (2015) and our recalculated WSIC estimates

345   for SO136-111 can provide insights into the magnitude of estimation differences. Generally

346   speaking, the GAM estimation produced higher WSIC estimates than the MAT (e.g., ~50% WSIC

347   at 23 ka BP while the MAT produced ~37% for the same time period); however, we believe it is

348   unlikely that statistical approaches alone could explain a larger difference (i.e., 50%) between

349   E27-23 and TAN1302-96.

350   The second possible explanation involves lateral sediment redistribution and focusing by

351   the ACC. We estimated sediment focusing for E27-23 using ^{230}Th data from Bradtmiller et al.

352   (2009) together with dry bulk density estimated using calcium carbonate content (Froelich,

353   1991). Both sedimentation rates and focusing factors (FF) for the E27-23 are relatively high

354   (max. = ~35 cm ka^{-1} and 26, respectively) during the LGM and Holocene, which could influence

355   the reliability of WSIC and SSST estimation (see Figure B2 in Appendix B). Several peaks in

356   focusing occurring around 16, 12, and 3 ka BP appear to closely correspond to periods of peak

357 WSIC (~67%, ~54%, and ~35%, respectively), suggesting a possible link. Lateral redistribution

358 could artificially increase or decrease relative abundances of some diatom groups, which could

359 lead to over- or under-estimations of sea ice coverage. Thorium analysis for TAN1302-96 is

360 beyond the scope of this study; however, future work could help address this uncertainty.

361 Although we are unable to identify the specific cause of the differences, we suggest

362 considering the results from all cores when drawing conclusions of regional sea ice history.

363

364 **4.2 The Role of Sea Ice on Early CO_2 Drawdown**

365 Kohfeld & Chase (2017) hypothesized that the initial drawdown of atmospheric CO_2 (~35

366 ppm) during the glacial inception of MIS 5d (~115 to 100 ka BP) was primarily driven by sea ice

367 capping and a corresponding stratification of surface waters, which reduced the CO_2 outgassing

368 of upwelled carbon-rich waters. This hypothesis is supported by several lines of evidence,

369 including: [1] sea salt sodium (ssNA) archived in Antarctic ice cores, suggesting sea ice

370 expansion near the Antarctic continent (Wolf et al., 2010); [2] $\delta^{15}N$ proxy data from the central

371 Pacific sector of the Southern Ocean, suggesting increased stratification south of the modern-

372 day Antarctic Polar Front (Studer et al., 2015); and [3] diatom assemblages in the Permanent

373 Open Ocean Zone (POOZ) of the Atlantic sector, suggesting a slight cooling and northward

374 expansion of sea ice during MIS 5d (Bianchi & Gersonde, 2002). Our data address this

375 hypothesis by providing insights into early sea ice expansion into the polar frontal zone of the

376 western Pacific sector.

377 Our data show that, in contrast to the Atlantic sector (Bianchi & Gersonde, 2002), there

378 does not appear to be any evidence of sea ice expansion in the southwestern Pacific during MIS

379 5d at either the TAN1302-96 or SO136-111 core sites (Figure 5). Unfortunately, the lack of

380 spatially extensive quantitative records extending back to Termination II limits our ability to

381 estimate the timing and magnitude of sea ice changes for regions poleward of 59°S in the

382 southwestern Pacific. We anticipate, however, that an advance in the sea ice edge, consistent

383 with those outlined in Bianchi and Gersonde (2002), likely would have reduced local SST as the

384 sea ice edge advanced closer to the core site. Indeed, the TAN1302-96 SSST record does show a

385 decrease to ~2°C (observed at 108 ka BP), which quickly rebounded to ~4°C by ~102 ka BP

386 (Figure 5). However, this SSST drop occurred roughly 7 ka BP after the initial CO_2 reduction,

387 suggesting that the CO_2 drawdown event and local SSST reduction may not be linked. Thus,

388 while we cannot rule out the possibility of modest sea ice advances or consolidation of pre-

389 existing sea ice (particularly to the south of the core sites), the quantitative WSI and SSST

390 reconstructions suggest that sea ice cover over our core site was limited during glacial

391 inception.

392 Given that sea ice was not at its maximum extent during the early glacial, it stands to

393 reason that any reductions to air-sea gas exchange in response to the hypothetically expanded

394 sea ice would not have been at its maximum impact either. Previous modeling work has

395 suggested that the maximum impact of sea ice expansion on glacial-interglacial atmospheric

396 CO_2 reductions ranged from 5 to 14 ppm (Kohfeld and Ridgwell, 2009). More recent modeling

397 studies are consistent with this range, suggesting a 10 ppm reduction (Stein et al., 2020), while

398 some studies even suggest a possible increase in atmospheric CO_2 concentrations due to sea ice

399 expansion (Khatiwala et al., 2019). Furthermore, Stein et al. (2020) suggest that the effects of

400 sea ice capping would have taken place after changes in deep ocean stratification had occurred

401 and would have contributed to CO_2 drawdown later during the mid-glacial period. These model

402 results, when combined with our data, suggest that even if modest sea ice advances did take

403 place during the early glacial (i.e., MIS 5d), their impacts on CO_2 variability likely would have

404 been modest, ultimately casting doubt on the hypothesis that early glacial CO_2 reductions of 35

405 ppm can be linked solely to the capping and stratification effects of sea ice expansion.

406

407 **4.3 Other Potential Contributors to Early Glacial CO_2 Variability**

408 The changes observed in WSIC and SSST from TAN1302-96 suggest that sea ice

409 expansion was likely not extensive enough early in the glacial cycle for a sea ice capping effect

410 to be solely responsible for early atmospheric CO_2 drawdown. This leaves open the question of

411 what may have contributed to early drawdown of atmospheric CO_2. In terms of the ocean's

412 role, we highlight three contenders: [1] a potentially non-linear response between sea ice

413 coverage and CO_2 sequestration potential; [2] links between sea ice expansion and early

414 changes in global ocean overturning, and [3] the impact of cooling on air-sea disequilibrium in

415 the Southern Ocean.

416 The first possible explanation considers that not all sea ice has the same capacity to

417 facilitate or inhibit air-sea gas exchange. We previously suggested that because sea ice was not

418 at its maximum extent during MIS 5d, the contribution of sea ice on CO_2 sequestration would

419 likely not be at its maximum extent either. However, this assumes a linear relationship between

420 sea ice coverage and CO_2 sequestration potential. We know that different sea ice properties,

421 such as thickness and temperature, determine overall porosity, with thicker and colder sea ice

422 being less porous and more effective at reducing air-sea gas exchange compared to thinner and

423 warmer sea ice (Delille et al., 2014). It is therefore possible that if modest sea ice advances took

424 place closer to the Antarctic continent (and were therefore not captured by TAN1302-96), they

425 may have been more effective at reducing CO_2 outgassing either by experiencing some type of

426 reorganization or consolidation, or through a change in properties such as temperature or

427 thickness. It is also possible that sea ice coverage over some regions leads to more effective

428 capping, while in other regions sea ice growth contributes only to marginal reductions in air-sea

429 gas exchange. This, theoretically, could point to a non-linear response between sea ice

430 expansion and CO_2 sequestration potential, and thus modest sea ice growth around the

431 Antarctic continent could have contributed in part to the ~35 ppm initial CO_2 drawdown event.

432 While this is theoretical and cannot be adequately addressed in this analysis, it is worthy of

433 deeper consideration.

434 The second possible explanation involves changes in the global overturning circulation.

435 Kohfeld and Chase (2017) previously examined the timing of changes in $\delta^{13}C$ of benthic

436 foraminifera solely from the Atlantic basin and observed that the largest changes in the Atlantic

437 Meridional Overturning Circulation (AMOC) coincided with the mid-glacial reductions in

438 atmospheric CO_2 changes mentioned above. Subsequent work of O'Neill et al. (2020) examined

439 whole-ocean changes in $\delta^{13}C$ of benthic foraminifera and noted that the separation between

440 $\delta^{13}C$ values of abyssal and deep ocean waters – and therefore the isolation of the abyssal ocean

441 - was actually initiated between MIS 5d and MIS 5a (114 to 71 ka BP). Evidence for early

442 changes in abyssal circulation and reductions in deep-ocean overturning have also been

443   detected in Indian Ocean δ^{13}C records (Govin et al., 2009). More recently, Indian Ocean εNd

444   records (Williams et al., 2021) have suggested that the abyssal ocean may have responded to

445   sea ice changes around the Antarctic continent early in the glacial cycle, with colder and more

446   saline AABW forming as sea ice expanded near the continent. If indications of an early-glacial

447   response in the global ocean circulation in the Indo-Pacific are correct, these data may also

448   point to an elevated importance of sea ice near the Antarctic continent in triggering early,

449   deep-ocean overturning changes.

450   The third possible explanation involves changes in surface ocean temperature gradients

451   in the Southern Ocean, and how they could influence air-sea gas exchange. Several recent

452   studies have pointed to the importance of changes to air-sea disequilibrium as a key

453   contributor to CO_2 uptake in the Southern Ocean (Eggleston & Galbraith, 2018; Marzocchi &

454   Jansen 2019; Khatiwala et al. 2019). Khatiwala et al. (2019) suggested that modelling studies

455   have traditionally underrepresented (or neglected) the role of air-sea disequilibrium in

456   amplifying the impact of cooling on potential CO_2 sequestration in the mid-high southern

457   latitudes during glacial periods. They argue that when the full effects of air-sea disequilibrium

458   are considered, ocean cooling can result in a 44 ppm decrease due to temperature-based

459   solubility effects alone. They attributed this increased impact of SST to a reduction in sea-

460   surface temperature gradients explicitly in polar mid-latitude regions (roughly between 40° and

461   60° north and south). If we compare the SST gradients in the southwest Pacific sector over the

462   last glacial-interglacial cycle (Figure 6), we see an early cooling response between MIS 5e-d

463   corresponding to roughly half of the full glacial cooling, specifically in the cores located south of

464   the modern STF. While not quantified, Bianchi and Gersonde (2002) also described a weakening

465   of meridional SST gradients between the Subantarctic and Antarctic Zones during MIS 5d in the

466   Atlantic sector. Although this analysis is based on sparse data, our SSST reconstructions are

467   consistent with the notion that surface ocean cooling, a weakening of meridional SST gradients,

468   and changes to the overall air-sea disequilibrium could be responsible for at least some portion

469   of the early CO_2 drawdown. Further SST estimates from the region, and from the global ocean,

470   are needed to substantiate this hypothesis.
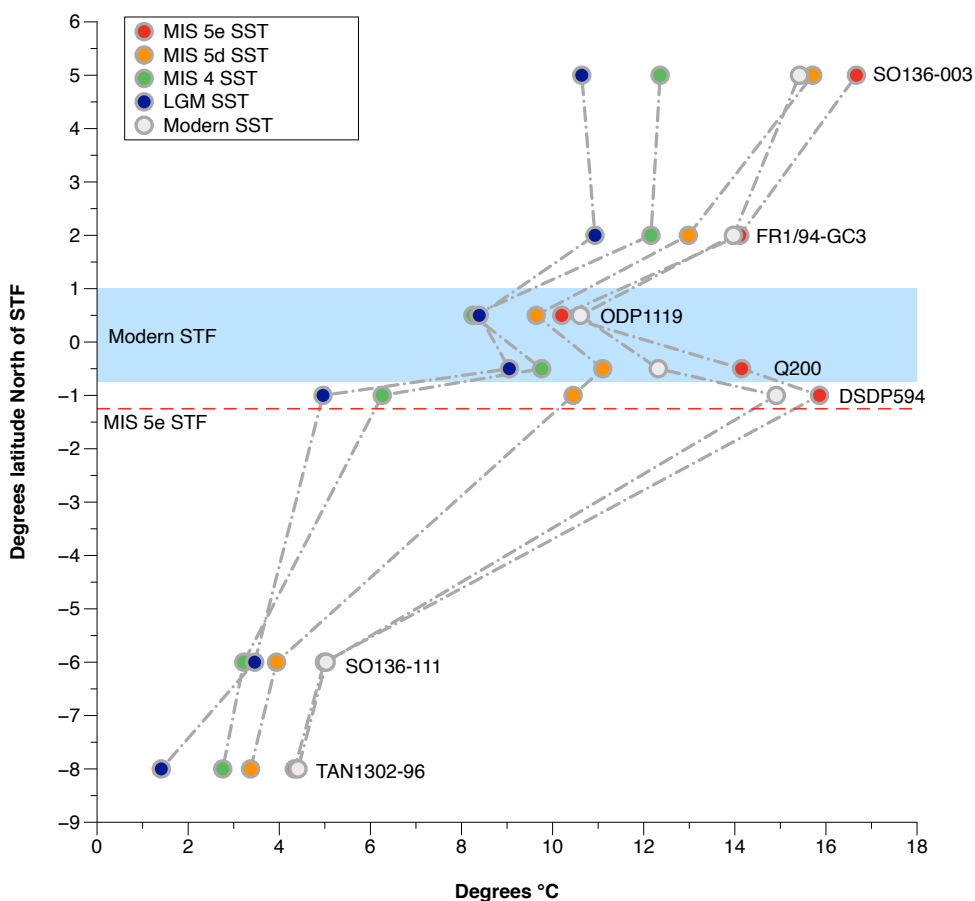
Figure 6: SST estimates from 7 cores located in the southwestern Pacific. SST used were 5-point averages (depending on sampling resolution) taken at MIS peaks/median dates in accordance with boundaries outlined in Lisiecki & Raymo, (2005). Due to the complex circulation and frontal structures in the region, cores were plotted in +/- distance from the average position of the modern STF. Cores used include: SO136-003 (SSTs calculated from alkenones, Pelejero et al., 2006); FR1/94-GC3 (alkenones, Pelejero et al., 2006); ODP 181-1119 (PF-MAT, Hayward et al., 2008); DSDP594 (PF-MAT, Schaefer et al., 2005); Q200 (PF-MAT, Weaver et al., 1998); SO136-111 (D-MAT, Crosta et al., 2004); and TAN1302-96 (D-MAT; *this study*). The blue band represents the modern STF zone while the red dotted line represents the southern shift in the STF during MIS 5e (Cortese et al., 2013).

4.4 Sea Ice Expansion and Ocean Circulation

Although the TAN1302-96 WSIC record suggests that sea ice was largely absent at the core site until the mid-glacial (~65 ka BP), the observed changes in sea ice could have modulated regional fluctuations in Antarctic Intermediate Water (AAIW) subduction throughout the glacial-interglacial cycle. The annual growth and decay of Antarctic sea ice plays

487   a critical role in regional water mass formation. Brine rejection results in net buoyancy loss in

488   regions of sea ice formation, while subsequent melt results in freshwater inputs and net

489   buoyancy gains near the ice margin (Shin et al., 2003; Pellichero et al., 2018). This increased

490   freshwater input and buoyancy gain near the ice margin can hinder AAIW subduction, with

491   direct and indirect impacts on both the upper and lower branches of the meridional

492   overturning circulation (Pellichero et al. 2018).

493   Previous research has used δ^{13}C in benthic foraminifera to track changes in the depth of

494   the interface between AAIW and Upper Circumpolar Deep Water (UCDW) (Pahnke and Zahn,

495   2005; Ronge et al., 2015). Low δ^{13}C values are linked to high nutrient concentrations found at

496   depths below ~1500 m in the UCDW, and higher δ^{13}C values are associated with the shallower

497   AAIW waters (Figure 5). Marine sediment core MD97-2120 (45.535°S, 174.9403°E, core depth

498   1210 m) was retrieved from a water depth near the interface between the AAIW and UCDW

499   water masses (Pahnke & Zahn, 2005). Over the last glacial-interglacial cycle, fluctuations in the

500   benthic δ^{13}C values from MD97-2120 suggest that the core site was intermittently bathed in

501   AAIW and UCDW, and that the vertical extent of AAIW fluctuated throughout the last glacial-

502   interglacial cycle. Ronge et al. (2015) used the δ^{13}C values from MD97-2120 and other core sites

503   to quantify the contributions of AAIW to the waters overlying MD97-2120 (%AAIW, Appendix

504   D). These results suggest that during warm periods, MD97- 2120 exhibited more positive δ^{13}C

505   values, corresponding to higher %AAIW, while cooler periods exhibited more negative values,

506   corresponding to lower %AAIW (Figure 5). This suggests that during cooler periods, the AAIW-

507   UCDW interface shoaled, reducing the total volume of AAIW and indirectly causing an

508   expansion of UCDW (Ronge et al., 2015).

509   Our comparison between %AAIW and regional WSIC estimates suggest a strong link

510   between the two (Figure 5). Specifically, we observe that AAIW shoaled and UCDW expanded

511   (i.e., %AAIW is low) during periods when sea ice expansion occurred. In contrast, during periods

512   of low WSIC, a reduced seasonal sea ice cycle, and warmer summer sea surface temperatures

513   (e.g., MIS 5e), %AAIW is observed to be high. This correlation supports the idea that increased

514   concentrations of regional sea ice resulted in a substantial summer freshwater flux into the

515   AAIW source region. This regional freshening likely promoted a shallower subduction of AAIW

516 and a corresponding volumetric expansion of UCDW, which can be seen by the isotopic offset

517 of the $\delta^{13}C$ values between the reference cores, and also by the increased carbonate dissolution

518 in MD97-2120 during glacial periods (Figure 7) (Pahnke et al., 2003; Ronge et al., 2015). These

519 findings directly link sea ice proxy records to observed changes in ocean circulation and water

520 mass geometry.

521

522
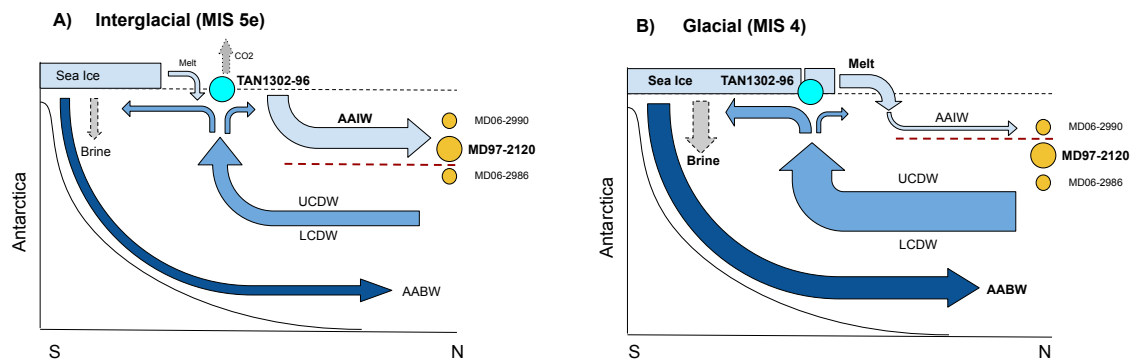
Figure 7: Schematic of changes in southwestern Pacific sector sea ice coverage and water mass
geometry between interglacial and glacial stages. **A)** Depicts interglacial conditions where sea
ice coverage is minimal and freshwater input from summer sea ice melt is low. This lack of
freshwater input allows AAIW to subduct to deeper depths and bath core MD97-2120,
capturing the higher $\delta^{13}C$ signature of the overlying AAIW waters. The AAIW-UCDW interface
(red dashed line) is located beneath MD97-2120. CO_2 outgassing is occurring as carbon-rich
Circumpolar Deep Waters upwell near Antarctica. **B)** Depicts glacial conditions where sea ice
expansion has occurred beyond TAN1302-96, increasing brine rejection, and stabilizing the
water column. As a result of the increased sea ice growth, subsequent summer melt increases
the freshwater flux into the AAIW source region and increases AAIW buoyancy. This buoyancy
gain shoals the AAIW-UCDW interface above core MD97-2120, causing the core site to be
bathed in low $\delta^{13}C$ UCDW. The shoaling of AAIW causes an indirect expansion of CDW,
increasing the glacial carbon stocks of the deep ocean while sea ice reduces CO_2 outgassing via
the capping mechanism.

537

538   In addition to its influence on regional freshwater forcing and AAIW reductions, these

539 sea ice changes may also coincide with larger-scale deep ocean circulation changes. The most

540 dramatic increases in winter sea ice observed in TAN1302-96 and SO136-111, along with

541 changes in %AAIW, are initiated during MIS 4. These shifts also correspond to basin-wide

542   changes in benthic $\delta^{13}C$ values in the Atlantic Ocean that suggest a shoaling in the AMOC during

543   MIS 4 (Oliver et al., 2010; Kohfeld & Chase, 2017). Changes in deep ocean circulation are also

544   recorded in ϵNd isotope data in the Indian sector of the Southern Ocean (Wilson et al., 2015),

545   suggesting extensive reductions in the AMOC during this period. Recent modelling literature

546   (Marzocchi & Jansen, 2019; Stein et al., 2020) suggests that sea ice formation directly impacts

547   marine carbon storage by increasing density stratification and reducing diapycnal mixing,

548   especially in simulations where brine rejection is enhanced near the Antarctic continental slope

549   and open ocean vertical mixing (and subsequent CO_2 outgassing) is reduced (Bouttes et al.

550   2010; 2012; Menviel et al. 2012). These simulations suggest a resulting CO_2 sequestration of

551   20-40 ppm into the deep ocean.

552   Taken collectively, the available data show that sea ice expansion, AAIW-UCDW

553   shoaling, changes in the AMOC, and a decrease in atmospheric CO_2 all occur concomitantly

554   during MIS 4 (Figure 5). It appears likely, therefore, that sea ice expansion during this time

555   influenced intermediate water density gradients through increased freshening and consequent

556   shoaling of AAIW, which may also have increased the efficiency of the carbon pump and

557   increased CO_2 uptake by phytoplankton (Sigman et al., 2021). This appears to have occurred

558   while simultaneously influencing deep-ocean density, and therefore stratification, through

559   brine rejection and enhanced deep water formation, which ultimately lead to decreased

560   ventilation (Abernathey et al., 2016). These changes in ocean stratification, combined with the

561   sea ice 'capping' mechanism, appear to agree with both the recent modelling efforts (Stein et

562   al., 2020) and observed proxy data, and fit well within the hypothesis that mid-glacial CO_2

563   variability was primarily the result of a more sluggish overturning circulation (Kohfeld & Chase,

564   2017).

565

566   **5.0 Summary & Conclusion**

567   This study presents new WSIC and SSST estimates from marine core TAN1302-96,

568   located in the southwestern Pacific sector of the Southern Ocean. We find that the WSIC

569   remained low during the early glacial cycle (130 to 70 ka BP), expanded during the middle

570   glacial cycle (~65 ka BP), and reached its maximum just prior to the LGM (~24.5 ka BP). These

571   results largely agree with nearby core SO136-111 but display some differences in WSIC

572   magnitude with E27-23. This discrepancy may be explained by differences in statistical

573   applications and/or lateral sediment redistribution, although more analysis is required to

574   determine the exact cause(s).

575   The lack of changes in SSST and the absence of winter sea ice over the core site during

576   the early glacial suggests that the sea ice capping mechanism and corresponding surface

577   stratification in this region is an unlikely cause for early CO_2 drawdown, and that alternative

578   hypotheses should be considered when evaluating the mechanism(s) responsible for the initial

579   drawdown. More specifically, we consider the impact of changes in SSST gradients between

580   ~40˚ to 60˚S and support the idea that changes in air-sea disequilibrium associated with

581   reduced sea-surface temperature gradients could be a potential mechanism that contributed to

582   early glacial reductions in atmospheric CO_2 concentrations (Khatiwala et al., 2019). Another key

583   consideration is the potentially non-linear response between sea ice expansion and CO_2

584   sequestration potential (i.e., that not all sea ice is equal in its capacity to sequester carbon).

585   More analyses are required to adequately address this.

586   We also observe a strong link between regional sea ice concentrations and vertical

587   fluctuations in the AAIW-UCDW interface. Regional sea ice expansion appears to coincide with

588   the shoaling of AAIW, likely due to the freshwater flux from summer sea ice melt increasing

589   buoyancy in the AAIW formation region. Furthermore, major sea ice expansion and AAIW

590   shoaling occurs during the middle of the glacial cycle and is coincident with previously

591   recognized shoaling in AMOC and mid-glacial atmospheric CO_2 reductions, suggesting a

592   mechanistic link between sea ice and ocean circulation.

593   In conclusion, this paper has focused exclusively on sea ice as a driver of physical

594   changes, but we recognize that these changes in sea ice will be accompanied by multiple

595   processes that interact and compete with each other. Marzocchi & Jansen (2019) note that

596   teasing apart the individual components of CO_2 fluctuations is complicated because of

597   interactions between sea ice capping, air-sea disequilibrium, AABW formation rates, and the

598   biological pump. We recognize that these processes may not act independently, and as such,

599 have contributed new data to help advance our collective understanding of the role of sea ice

600 on influencing atmospheric CO_2 variability on a glacial-interglacial time scale.

601

602 **6.0 Appendices**

603 **Appendix A: Age Model & Sampling Depths**

604 **Table A1:** Radiocarbon dates taken from TAN1302-96. NDFB = Not Distinguishable from Background
605

Lab Code	Sample Material	Core Name	Depth (cm)	δ13C (per mil)	δ13C (+/-)	% Modern Carbon	1σ error	Fraction Modern	(+/-)	Radiocarbon Year	1σ error	Reference
NZA 57105	*N. pachyderma* and *G. bulloides*	TAN1302-96	21	1	0.2	/	/	0.5982	0.0018	4127	24	Prebble et al., 2017
NZA 57109	*N. pachyderma* and *G. bulloides*	TAN1302-96	50	0.7	0.2	/	/	0.3723	0.0015	7936	32	Prebble et al., 2017
OZX 517	*N. pachyderma* and *G. bulloides*	TAN1302-96	63	1	0.1	30.62	0.15	/	/	9505	40	*This study*
NZA 61429	*N. pachyderma* and *G. bulloides*	TAN1302-96	75	0.7	0.2	/	/	0.2373	0.0011	11554	37	Prebble et al., 2017
OZX 518	*N. pachyderma* and *G. bulloides*	TAN1302-96	87	-0.1	0.1	19.62	0.11	/	/	13085	45	*This study*
OZX 519	*N. pachyderma* and *G. bulloides*	TAN1302-96	130	1.7	0.1	0.02	0.04	/	/	NDFB	/	*This study*
OZX 520	*N. pachyderma* and *G. bulloides*	TAN1302-96	170	-1.1	0.3	0.03	0.04	/	/	NDFB	/	*This study*

606
607 **Table A2:** Tie points used in construction of the TAN1302-96 age model
608

TAN1302-96 Depth (cm)	TAN1302-96 δ18O	LR04 Age	LR04 δ18O
110	4.710	18000	5.02
170	3.930	56000	4.35
200	3.782	70000	4.32
220	3.07	82000	3.8
230	3.23	87000	4.18
250	3.22	109000	4.12
270	2.90	123000	3.1
300	3.660	129000	3.9
320	4.350	140000	4.98

609

610 **Table A3:** Sample depth and corresponding age. Diatom slides using Method 1 used sediment samples that are
611 even (e.g., 10, 20, 30, etc.), while diatom slides using Method 2 used sediment samples that are odd (e.g., 53, 87,
612 etc.). * Indicates the sample was calculated based on linear sedimentation rates.
613

Sample Depth (cm)	Age	Sample Depth (cm)	Age	Sample Depth (cm)	Age	Sample Depth (cm)	Age
10	1001*	100	16011	197	68608	260	116007
20	2531*	103	16609	200	69999	263	118110
30	4061	107	17406	203	71790	267	120912
40	5591	110	18000	207	74196	270	123000
50	7152	113	19893	210	76000	273	123597
53	7584	117	22434	213	77802	277	124398
57	8108	120	24340	217	80207	280	124998
60	8486	123	26244	220	82000	283	125598
63	8890	127	28780	223	83491	287	126398
67	9735	130	30686	227	85503	290	126999
70	10404	140	37035	230	87000	293	127600
73	11056	150	43357	233	90289	297	128403
77	11844	160	49677	237	94703	300	129000
80	12306	170	56000	240	98011	303	130644
83	12747	180	60672	243	101314	307	132850
87	13361	183	62074	247	105715	310	134503
90	13963	187	63942	250	108999	313	136155
93	14581	190	65340	253	111094	317	138360
97	15404	193	66740	257	113903	320	140000

614

Appendix B: Diatom Slide Preparation Comparison
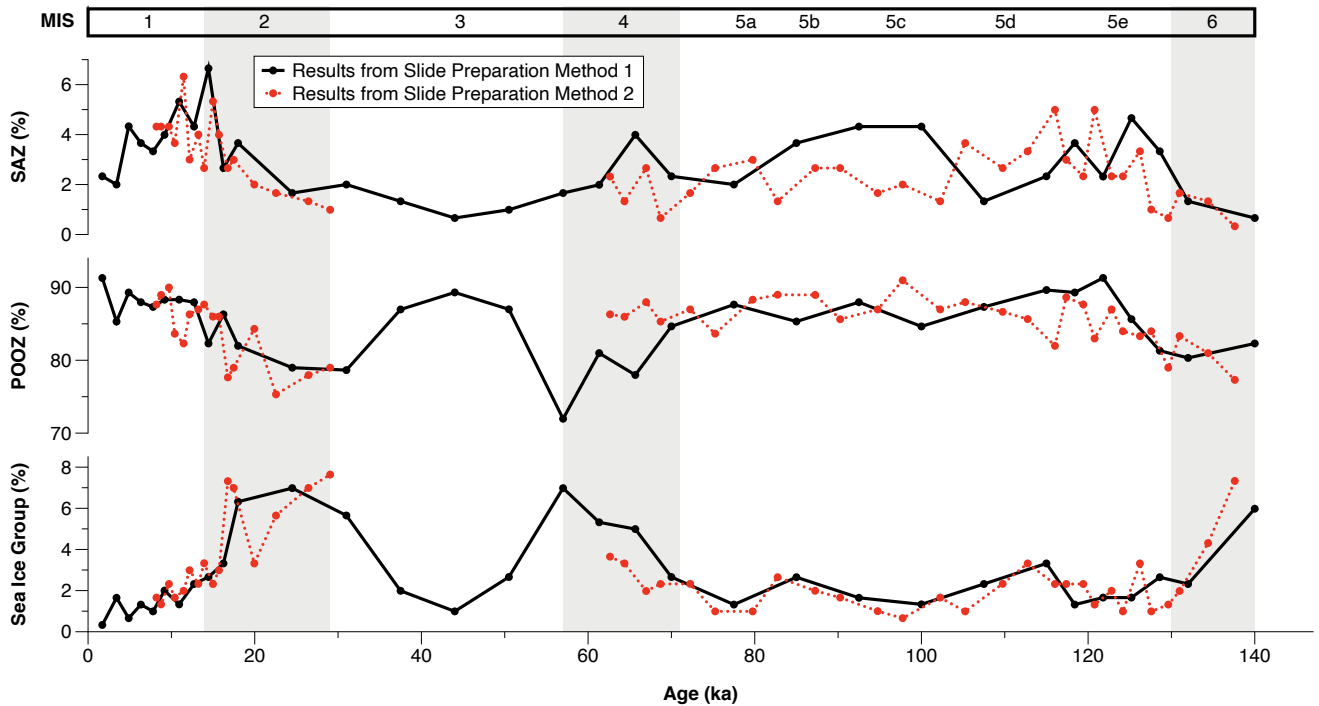
Figure B1: Results from diatom slide preparation methods 1 & 2. No notable differences or biases were observed between the two different methods.

Appendix C: TAN1302-96 and E27-23 Comparison

Potential Causes for WSIC Estimate Differences

The third potential cause for the observed differences between TAN1302-96 and E27-23 WSIC estimates is through the cumulative effects of different laboratory protocols. While it is difficult to determine precisely how much different laboratory protocols could influence the results, we cannot exclude this explanation as a possible contributor to differences in WSIC.

The fourth potential cause for differences in WSIC estimates between E27-23 and TAN1302-96 are differences in counting and identification methods. We believe this is an unlikely cause for the differences observed between E27-23 and TAN1302-96 primarily because of the magnitude of counting discrepancies required to cause a difference of 50% WSIC estimates between the two cores. The close coupling of WSIC estimates between TAN1302-96 and SO136-111 over the entire glacial-interglacial cycle supports that a fundamental issue

632   relating to taxonomic identification and/or methodology is an unlikely explanation for the

633   observed WSIC differences.

634   Finally, the fifth potential cause of differing WSIC estimates is selective diatom

635   preservation (e.g., Pichon et al., 1999; Ragueneau et al., 2000). The similarities between

636   TAN1302-96 and SO136-111 WSIC estimates, along with independent indicators in cores E27-23

637   and TAN1302-96, suggest that this is unlikely. For E27-23, Bradtmiller et al. (2009) used the

638   consistent relationship between ^{231}Pa/^{230}Th ratios and opal fluxes to suggest that dissolution

639   remained relatively constant between the LGM and Holocene periods. In TAN1302-96, we

640   assigned a semi-quantitative diatom preservation value between 1 (extreme dissolution) and 4

641   (virtually perfect preservation) for each counted specimen. The average preservation of

642   diatoms for the entire core was 3.38 ± 0.13, with no observed bias based on sedimentation rate

643   or MIS. This assessment, although semi-qualitative, suggests that preservation remained

644   relatively constant (and good) throughout TAN1302-96, and is therefore unlikely to cause large

645   differences in WSIC between the two cores.
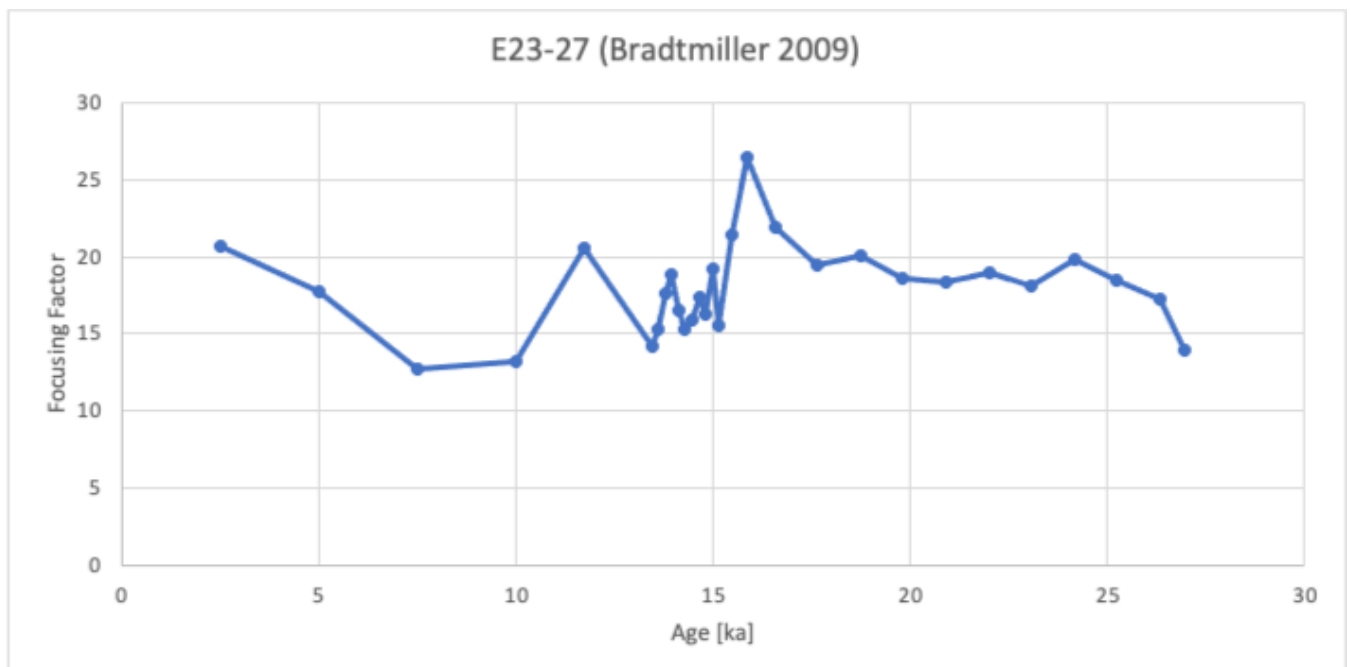
646
647   **Figure C1:** Preliminary focusing factor (FF) values for E27-23. These results suggest notable lateral sediment
648   redistribution over the last 26 ka BP, requiring further analysis (Bradtmiller et al., 2009).
649

Appendix D: %AAIW Calculation

The calculation of %AAIW in this study is the same as was used in Ronge et al. (2015):

$$\%AAIW = (\delta^{13}C_{MD97\text{-}2120} - \delta^{13}C_{MD06\text{-}2986}) / (\delta^{13}C_{MD06\text{-}2990} - \delta^{13}C_{MD06\text{-}2986}) * 100$$

All core information for MD97-2120, MD06-2986, and MD06-2990, along with supporting supplemental information can be found through the original publication.

7.0 Data Availability

All data has been published on Pangaea and can be found at:

https://doi.pangaea.de/10.1594/PANGAEA.938457.

8.0 Author Contributions

The authors confirm that the contributions to this paper are as follows: study conception and design: KK, HB; author data collection: JJ, KK, HB, XC, ML, GD, ZC, AL; analysis and interpretation of results: JJ, KK, HB, XC, ZC, AL, HA, GJ; draft manuscript preparation and/or editing: JJ, KK, HB, XC, GD, ZC, AL, HA, GJ. All authors reviewed the results and approved the final version of the manuscript.

9.0 Competing Interests

The authors declare that they have no conflict of interest.

10.0 Acknowledgements

This work was supported by a Canadian Natural Sciences and Engineering Research Council grant (Discovery Grant RGPIN342251) to Karen Kohfeld. Travel funding for workshop collaboration was provided to Jacob Jones by a Past Global Changes (PAGES) grant to the Cycles of Sea Ice Dynamics in the Earth System (C-SIDE) Working Group. Rachel Meyne (Colgate University) assisted with slide preparation; Maureen Soon (University of British Columbia)

assisted with opal concentration measurements; Marlow Pellatt (Parks Canada) assisted with

project conceptualization and guidance. The TAN1302-96 core was collected during the

TAN1302 RV Tangaroa voyage to the Mertz Polynya. We would like to thank the Voyage leader

Dr. Mike Williams and Captain Evan Solly and the crew, technicians and scientists involved in

the TAN1302 voyage. The voyage was co-funded by NIWA, Australian, and French research

funding. We acknowledge Dr. Andrew Kingston for running the stable isotopes at NIWA. We

acknowledge ANSTO grant AP11676 for funding the additional radiocarbon dates. This research

was partially supported by the Australian Government through the Australian Research

Council's Discovery Projects funding scheme (project DP180102357, awarded to Zanna Chase

and Helen Bostock).

11.0 References

Abernathey, R. P., Cerovecki, I., Holland, P. R., Newsom, E., Mazloff, M., and Talley, L. D.: Water-mass transformation by sea ice in the upper branch of the Southern Ocean overturning. Nat. Geosci., 9, 596–601, https://doi.org/10.1038/ngeo2749, 2016.

Archer, D.E., Martin, P.A., Milovich, J., Brovkin, V., Plattner, G.K., and Ashendel, C.: Model sensitivity in the effect of Antarctic sea ice and stratification on atmospheric pCO2. Paleoceanography, 18, 1012, https://doi.org/10.1029/2002PA000760, 2003.

Benz, V., Esper, O., Gersonde, R., Lamy, F., and Tiedemann, R.: Last Glacial Maximum sea surface temperature and sea-ice extent in the Pacific sector of the Southern Ocean. Quaternary Sci. Rev., 146, 216–237, https://doi.org/10.1016/j.quascirev.2016.06.006, 2016.

Bianchi, C., and Gersonde, R.: The Southern Ocean surface between Marine Isotope Stages 6 and 5d: shape and timing of climate changes. Palaeogeogr., Palaeoclimatol., Palaeoecol., 187, 151–177, https://doi.org/10.1016/S0031-0182(02)00516-3, 2002.

Bereiter, B., Eggleston, S., Schmitt, J., Nehrbass-Ahles, C., Stocker, T.F., Fischer, H., Kipfstuhl, S., and Chappellaz, J.: Revision of the EPICA Dome C CO2 record from 800 to 600 kyr before present. Geophys. Research Lett., 42: 542–549, https://doi.org/10.1002/2014GL061957, 2015.

Bostock, H., Hayward, B., Neil, H., Sabaa, A., & Scott, G.: Changes in the position of the Subtropical Front south of New Zealand since the last glacial period. Paleoceanography, 30, 824–844, https://doi.org/10.1002/2014PA002652, 2015.

715 Bouttes, N., Paillard, D., and Roche, D. M.: Impact of brine-induced stratification on the glacial
716 carbon cycle. Clim. Past, 6, 575–589. https://doi.org/10.5194/cp-6-575-2010, 2010.

718 Bouttes, N., Paillard, D., Roche, D. M., Waelbroeck, C., Kageyama, M., Lourantou, A., Michel, E.,
719 and Bopp, L.: Impact of oceanic processes on the carbon cycle during the last termination, Clim.
720 Past, 8, 149–170, https://doi.org/10.5194/cp–8-149-2012, 2012

722 Bradtmiller, L.I., Anderson, R.F., Fleisher, M.Q. and Burckle, L.H.: Comparing glacial and
723 Holocene opal fluxes in the Pacific sector of the Southern Ocean, Paleoceanography, 24,
724 PA2214, https://doi.org/10.1029/2008PA001693, 2009.

726 Butzin, M., Köhler, P., and Lohmann, G.: Marine radiocarbon reservoir age simulations for the
727 past 50,000 years, Geophys. Research Lett., 44, 8473–8480,
728 https://doi.org/10.1002/2017GL074688, 2017.

730 Butzin, M., Heaton, T.J., Köhler, P., and Lohmann, G.: A short note on marine reservoir age
731 simulations used in INTCAL20, Radiocarbon, 62, 1–7, https://doi.org/10.1017/RDC.2020.9,
732 2020.

734 Cefarelli, A.O., Ferrario, M.E., Almandoz, G.O., Atencio, A.G., Akselman, R., and Vernet, M.:
735 Diversity of the diatom genus Fragilariopsis in the Argentine Sea and Antarctic waters:
736 morphology, distribution, and abundance. Polar Biol., 33, 1463–1484,
737 https://doi.org/10.1007/s00300-010-0794-z, 2010.

739 Cortese, G., Dunbar, G. B., Carter, L., Scott, G., Bostock, H., Bowen, M., Crundwell, M., Hayward,
740 B. W., Howard, W., Martínez, J. I., Moy, A., Neil, H., Sabaa, A., and Sturm, A.: Southwest Pacific
741 Ocean response to a warmer world: Insights from Marine Isotope Stage
742 5e, Paleoceanography, 28, 585–598, https://doi.org/10.1002/palo.20052, 2013.

744 Crosta, X., Pichon, J.-J., and Burckle, L.H.: Application of modern analog technique to marine
745 Antarctic diatoms: reconstruction of maximum sea-ice extent at the Last Glacial Maximum,
746 Paleoceanography, 13, 284–297, https://doi.org/10.1029/98PA00339, 1998.

748 Crosta, X., Sturm, A., Armand, L., and Pichon, J.-J.: Late Quaternary sea ice history in the Indian
749 sector of the Southern Ocean as recorded by diatom assemblages. Mar. Micropaleontol., 50,
750 209–223, https://doi.org/10.1016/S0377-8398(03)00072-0, 2004.

752 Crosta, X., Shukla, S.K., Ther, O., Ikehara, M., Yamane, M., and Yokoyama, Y.: Last Abundant
753 Appearance Datum of Hemidiscus karstenii driven by climate change. Mar.
754 Micropaleontol., 157, 101861, https://doi.org/10.1016/j.marmicro.2020.101861, 2020.

756 Delille, B., Vancoppenolle, M., Geilfus, N.X., Tilbrook, B., Lannuzel, D., Schoemann, V.,
757 Becquevort, S., Carnat, G., Delille, D., Lancelot, C., Chou, L., Dieckmann, G.S., and Tison, J.L.:

758   Southern Ocean CO_2 sink: The contribution of sea ice, J. Geophys. Res., 119, 6340-3655,
759   https://doi.org/10.1002/2014JC009941, 2014.
760
761   Eggleston, S., and Galbraith, E.D.: The devil's in the disequilibrium: multi-component analysis of
762   dissolved carbon and oxygen changes under a broad range of forcings in a general circulation
763   model, Biogeosciences 15, 3761-3777, https://doi.org/10.5194/bg-15-3761-2018, 2018.
764
765   Esper, O., Gersonde, R., and Kadagies, N.: Diatom distribution in southeastern Pacific surface
766   sediments and their relationship to modern environmental variables, Palaeogeogr.,
767   Palaeoclimatol., Palaeoecol., 287, 1–27. https://doi.org/10.1016/j.palaeo.2009.12.006, 2010.
768
769   Esper, O., and Gersonde, R.: New tools for the reconstruction of Pleistocene Antarctic Sea ice,
770   Palaeogeogr., Palaeoclimatol., Palaeoecol., 399, 260–283,
771   https://doi.org/10.1016/j.palaeo.2014.01.019, 2014a.
772
773   Esper, O., & Gersonde, R.: Quaternary surface water temperature estimations: New diatom
774   transfer functions for the Southern Ocean, Palaeogeogr., Palaeoclimatol., Palaeoecol., 414, 1–
775   19, https://doi.org/10.1016/j.palaeo.2014.08.008, 2014b.
776
777   Fenner, J., Schrader, H., and Wienigk, H. (Eds.): Diatom Phytoplankton Studies in the Southern
778   Pacific Ocean, Composition and Correlation to the Antarctic Convergence and Its
779   Paleoecological Significance, Geologisch-Paläontologisches Institut and Museum der Universität
780   Kiel, Germany, 1976.
781
782   Ferrari, R., Jansen, M.F., Adkins, J.F., Burke, A., Stewart, A.L., Thompson, A.F.: Antarctic sea ice
783   control on ocean circulation in present and glacial times, P. Natl. Acad. Sci. USA., 111, 8753–
784   8758, https://doi.org/10.1073/pnas.1323922111, 2014.
785
786   Ferry, A.J., Crosta, X., Quilty, P.G., Fink, D., Howard, W., and Armand, L.K.: First records of
787   winter sea ice concentration in the southwest Pacific sector of the Southern
788   Ocean, Paleoceanography, 30, 1525–1539, https://doi.org/10.1002/2014pa002764, 2015.
789
790   Froelich, P. N.: Biogenic opal and carbonate accumulation rates in the Subantarctic South
791   Atlantic: The late Neogene of Meteor Rise site 704, Proceedings of the Ocean Drilling Program,
792   Scientific Results, 120, 515–549, 1991.
793
794   Fryxell, G.A., and Hasle, G.R.: The genus Thalassiosira: some species with a modified ring of
795   central strutted processes, Nova Hedwigia Beihefte, 54, 67-98, 1976.
796
797   Fryxell, G.A., and Hasle, G.R.: The marine diatom Thalassiosira oestrupii: structure, taxonomy
798   and distribution, Am. J. Bot., 67, 804-814, 1980.
799
800   Galbraith, E., and de Lavergne, C.: Response of a comprehensive climate model to a broad
801   range of external forcings: relevance for deep ocean ventilation and the development of late

802   Cenozoic ice ages, Clim. Dynm., 52, 653–679, https://doi.org/10.1007/s00382-018-4157-8,
803   2019.
804
805   Gersonde, R., and Zielinski, U.: The reconstruction of late Quaternary Antarctic sea-ice
806   distribution—the use of diatoms as a proxy for sea-ice, Palaeogeogr., Palaeoclimatol.,
807   Palaeoecol., 162, 263–286, https://doi.org/10.1016/S0031-0182(00)00131-0, 2000.
808
809   Gersonde, R., Crosta, X., Abelmann, A., and Armand, L.: Sea-surface temperature and sea ice
810   distribution of the Southern Ocean at the EPILOG last Glacial Maximum—a circum-Antarctic
811   view based on siliceous microfossil records, Quaternary Sci. Rev., 24, 869–896,
812   https://doi.org/10.1016/j.quascirev.2004.07.015, 2005.
813
814   Ghadi, P., Nair, A., Crosta, X., Mohan, R., Manoj, M.C, and Meloth, T.: Antarctic sea-ice and
815   palaeoproductivity variation over the last 156,000 years in the Indian sector of Southern
816   Ocean, Mar. Micropaleontol., 160, 101894. https://doi.org/10.1016/j.marmicro.2020.101894,
817   2020.
818
819   Govin, A., Michel, E., Labeyrie, L., Waelbroeck, C., Dewilde, F., and Jansen, E.: Evidence for
820   northward expansion of Antarctic Bottom Water mass in the Southern Ocean during the last
821   glacial inception, Paleoceanography, 24, PA1202, doi:10.1029/2008PA001603, 2009.
822
823   Guiot, J., de Beaulieu, J.L., Chceddadi, R., David, F., Ponel, P., Reille, M.: The climate of western
824   Europe during the last Glacial/Interglacial cycle derived from pollen and insect remains,
825   Palaeogeogr., Palaeoclimatol., Palaeoecol., 103, 73–93, https://doi.org/10.1016/0031-
826   0182(93)90053-L, 1993.
827
828   Guiot, J., and de Vernal, A.: Is spatial autocorrelation introducing biases in the apparent
829   accuracy of paleoclimatic reconstructions? Quaternary Sci. Rev., 30, 1965–1972,
830   https://doi.org/10.1016/j.quascirev.2011.04.022, 2011.
831
832   Hasle G.R., and Syvertsen, E.E.: Marine diatoms. In: Tomas CR (Eds.) Identifying marine
833   phytoplankton. Academic Press, 5–385, 1997.
834
835   Heaton, T., Köhler, P., Butzin, M., Bard, E., Reimer, R., Austin, W., Bronk Ramsey, C., Grootes, P.,
836   Hughen, K., Kromer, B., Reimer, P., Adkins, J., Burke, A., Cook, M., Olsen, J., and Skinner, L.:
837   Marine20—The Marine Radiocarbon Age Calibration Curve (0–55,000 cal. BP), Radiocarbon, 62,
838   779–820, https://doi.org/10.1017/RDC.2020.68, 2020.
839
840   Johansen, J.R., and Fryxell, G.A.: The genus Thalassiosira (Bacillariophyceae): studies on species
841   occurring south of the Antarctic Convergence Zone, Deep-Sea Res. Pt. B. Oceanogr Lit Rev, 32,
842   1050, https://doi.org/10.1016/0198-0254(85)94033-6, 1985.
843

844 Khatiwala, S, Schmittner, A, and Muglia, J.: Air-sea disequilibrium enhances ocean carbon
845 storage during glacial periods. Science Advances, 5(6), eaaw4981–eaaw4981.
846 https://doi.org/10.1126/sciadv.aaw4981, 2019.

848 Kohfeld, K.E., and Chase, Z.: Temporal evolution of mechanisms controlling ocean carbon
849 uptake during the last glacial cycle, Earth Planet Sc. Lett, 472, 206–215,
850 https://doi.org/10.1016/j.epsl.2017.05.015, 2017.

852 Kohfeld, K.E., and Ridgwll, A.: Glacial-Interglacial Variability in Atmospheric CO_2 – Surface
853 Ocean-Lower Atmospheric Processes (American Geophysical Union), edited by: Quéré, C. L. and
854 Saltzman, E. S), Washington D.C, USA, https://doi.org/10.1029/2008GM000845, 2009.

856 Lhardy, F., Bouttes, N., Roche, D. M., Crosta, X., Waelbroeck, C., and Paillard, D.: Impact of
857 Southern Ocean surface conditions on deep ocean circulation during the LGM: a model analysis,
858 Clim. Past, 17, 1139–1159, https://doi.org/10.5194/cp-17-1139-2021, 2021.

860 Lisiecki, L.E., and Raymo, M.E.: A Pliocene–Pleistocene stack of 57 globally dis- tributed benthic
861 δ^{18}O records. Paleoceanography, 20, 1-17, https://doi.org/10.1029/2004PA001071, 2005.

863 Locarnini, R.A., Mishonov, A.V., Antonov, J.I., Boyer, T.P., Garcia, H.E., Baranova, O.K., Zweng,
864 M.M., Paver, C.R., Reagan, J.R., Johnson, D.R., Hamilton, M., and Seidov, D.: World Ocean atlas,
865 In: Levitus, S. (Ed.), A. Mishonov Technical, 40, http://doi.org/10.7289/V55X26VD, 2013.

867 Lougheed, B. C., and Obrochta, S. P.: A Rapid, Deterministic Age-Depth Modeling Routine for
868 Geological Sequences With Inherent Depth Uncertainty, Paleoceanography and
869 Paleoclimatology, 34, 122–133. https://doi.org/10.1029/2018PA003457, 2019.

871 Marzocchi, A., and Jansen, M.F.: Global cooling linked to increased glacial carbon storage via
872 changes in Antarctic sea ice, Nat. Geosci., 12, 1001–1005. https://doi.org/10.1038/s41561-019-
873 0466-8, 2019.

875 Menviel, L., Joos, F., and Ritz, S.: Simulating atmospheric CO_2, ^{13}C and the marine carbon cycle
876 during the Last Glacial–Interglacial cycle: possible role for a deepening of the mean
877 remineralization depth and an increase in the oceanic nutrient inventory, Quaternary Sci.
878 Rev., 56, 46–68, https://doi.org/10.1016/j.quascirev.2012.09.012, 2012.

880 Mix, A.C., Bard, E., & Schneider, R.: Environmental processes of the ice age: land, oceans,
881 glaciers (EPILOG), Quaternary Sci. Rev, 20, 627–657, https://doi.org/10.1016/S0277-
882 3791(00)00145-1, 2001.

884 Morales Maqueda, M.A., and Rahmstorf, S.: Did Antarctic sea-ice expansion cause glacial CO2
885 decline? Geophysical Research Letters, 29, 11-1–11–3. https://doi.org/10.1029/2001GL013240,
886 2002.
887

888 Oliver, K. I. C., Hoogakker, B. A. A., Crowhurst, S., Henderson, G. M., Rickaby, R. E. M., Edwards,
889 N. R., and Elderfield, H.: A synthesis of marine sediment core δ 13 C data over the last 150 000
890 years. Clim. Past, 5, 2497–2554, https://doi.org/10.5194/cpd-5-2497-2009, 2009.
891

892 O'Neill, C.M., Hogg, A.M., Ellwood, M.J., Opdyke, B.N., & Eggins, S.M.: Sequential changes in
893 ocean circulation and biological export productivity during the last glacial–interglacial cycle: a
894 model–data study, Clim. Past, 17, 171–201, https://doi.org/10.5194/cp-17-171-2021, 2021.
895

896 Pahnke, K., Zahn, R., Elderfield, H., and Schulz, M.: 340,000-year centennial-scale marine record
897 of Southern Hemisphere climatic oscillation, Science, 301, 948–952,
898 https://doi.org/10.1126/science.1084451, 2003.
899

900 Pahnke, K., and Zahn, R.: Southern Hemisphere Water Mass Conversion Linked with North
901 Atlantic Climate Variability. Science, 307, 1741–1746, https://doi.org/10.1126/science.1102163,
902 2005.
903

904 Paterne, M., Michel, E., and Héros, V. : Variability of marine 14C reservoir ages in the Southern
905 Ocean highlighting circulation changes between 1910 and 1950, Earth Planet Sc. Lett., 511, 99–
906 104, https://doi.org/10.1016/j.epsl.2019.01.029f, 2019.
907

908 Pellichero, V., Sallée, J.B., Chapman, C., and Downes, S.: The Southern Ocean meridional
909 overturning in the sea-ice sector is driven by freshwater fluxes, Nat. Commun., 9, 1789,
910 https://doi.org/10.1038/s41467-018-04101-2, 2018.
911

912 Pichon, J.J., Bareille, G., Labracherie, M., Labeyrie, L.D., Baudrimont, A. & Turon, J.L.:
913 Quantification of the Biogenic Silica Dissolution in Southern Ocean Sediments, Quaternary
914 Res., 37, 361–378, https://doi.org/10.1016/0033-5894(92)90073-R, 1992.
915

916 Prebble, J. G., Bostock, H. C., Cortese, G., Lorrey, A. M., Hayward, B. W., Calvo, E., Northcote, L.
917 C., Scott, G. H., and Neil, H. L.: Evidence for a Holocene Climatic Optimum in the southwest
918 Pacific: A multiproxy study, Paleoceanography, 32, 763–779,
919 https://doi.org/10.1002/2016PA003065, 2017.
920

921 Ragueneau, O., Tréguer, P., Leynaert, A., Anderson, R.F., Brzezinski, M.A., DeMaster, D.J.,
922 Dugdale, R.C., Dymond, J., Fischer, G., François, R., Heinze, C., Maier-Reimer, E., Martin-
923 Jézéquel, V., Nelson, D.M., & Quéguiner, B.: A review of the Si cycle in the modern ocean:
924 recent progress and missing gaps in the application of biogenic opal as a paleoproductivity
925 proxy. Global Planet Change, 26, 317–365, https://doi.org/10.1016/S0921-8181(00)00052-7,
926 2000.
927

928 Renberg, I.: A procedure for preparing large sets of diatom slides from sediment cores, J.
929 Paleolimnol., 4, 87-90, https://doi.org/10.1007/bf00208301, 1990.
930

931   Reynolds, R., Rayner, N., Smith, T., Stokes, D., and Wang, W.: An Improved In Situ and Satellite
932   SST Analysis for Climate, J. Climate, 15, 1609–1625, https://doi.org/10.1175/1520-
933   0442(2002)015<1609:AIISAS>2.0.CO;2, 2002.

934

935   Reynolds, R., Smith, T., Chunying, L., Chelton, D., Casey, K., & Schlax, M.: Daily High-Resolution-
936   Blended Analyses for Sea Surface Temperature J. Climate, 20, 5473–5496,
937   https://doi.org/10.1175/2007JCLI1824.1, 2007.

938

939   Ronge, T.A., Steph, S., Tiedemann, R., Prange, M., Merkel, U., Nürnberg, D., and Kuhn, G.:
940   Pushing the boundaries: Glacial/interglacial variability of intermediate and deep waters in the
941   southwest Pacific over the last 350,000 years, Paleoceanography, 30, 23–38,
942   https://doi.org/10.1002/2014pa002727, 2015.

943

944   Rutgers van der Loeff, M.M., Cassar, N., Nicolaus, M., Rabe, B., and Stimac, I.: The influence of
945   sea ice cover on air-sea gas exchange estimated with radon-222 profiles, J. Geophys. Res.,
946   Oceans, 119, 2735–2751, https://doi.org/10.1002/2013jc009321, 2014.

947

948   Schlitzer, R. (2005). Interactive analysis and vizualization of geoscience data with Ocean Data
949   View, Comput. Geosci., 28, 1211–1218, https://doi.org/10.1016/S0098-3004(02)00040-7, 2005.

950

951   Schneider Mor, A., Yam, R., Bianchi, C., Kunz-Pirrung, M., Gersonde, R., & Shemesh, A. (2012).
952   Variable sequence of events during the past seven terminations in two deep-sea cores from the
953   Southern Ocean, Quaternary Res., 77, 317–325, https://doi.org/10.1016/j.yqres.2011.11.006,
954   2012.

955

956   Shin, S.I., Liu, Z., Otto-Bliesner, B., Kutzbach, J., & Vavrus, Stephen J.: Southern Ocean sea-ice
957   control of the glacial North Atlantic thermohaline circulation, Geophys. Res, Lett., 30, 1096,
958   https://doi.org/10.1029/2002GL015513, 2003.

959

960   Sigman, D., and Boyle, E.: Glacial/Interglacial variations in atmospheric carbon dioxide, Nature,
961   407, 859-869, https://doi.org/10.1038/35038000, 2000.

962

963   Sigman, D., Fripiat, F., Studer, A. S., Kemeny, P. C., Martínez-García, A., Hain, M. P., Ai, X., Wang,
964   X., Ren, H., and Haug, G. H.: The Southern Ocean during the ice ages: A review of the Antarctic
965   surface isolation hypothesis, with comparison to the North Pacific, Quaternary Sci. Rev., 254,
966   106732, https://doi.org/10.1016/j.quascirev.2020.106732, 2021.

967

968   Smith, R. O., Vennell, R., Bostock, H. C., & Williams, M. J.: Interaction of the subtropical front
969   with topography around southern New Zealand, Deep Sea Res. Part I Oceanogr. Res. Pap., 76,
970   13–26, https://doi.org/10.1016/j.dsr.2013.02.007, 2013.

971

972   Sokolov, S., & Rintoul, S.: Circumpolar structure and distribution of the Antarctic Circumpolar
973   Current fronts: 2. Variability and relationship to sea surface height. J. Geophys. Res.-
974   Oceans, 114, https://doi.org/10.1029/2008JC005248, 2009.

975
976 Stein, K., Timmermann, A., Kwon, E.Y., and Friedrich, T.: Timing and magnitude of Southern
977 Ocean sea ice/carbon cycle feedbacks, P. Natl. Acad Sci. USA, 117, 4498–4504,
978 https://doi.org/10.1073/pnas.1908670117, 2020.
979
980 Stephens, B.B., and Keeling, R.F.: The influence of Antarctic sea ice on glacial–interglacial CO_2
981 variations, Nature, 404, 171–174, https://doi.org/10.1038/35004556, 2000.
982
983 Studer, A. S., Sigman, D.M., Martínez-García, A., Benz, V., Winckler, G., Kuhn, G., Esper, O.,
984 Lamy, F., Jaccard, S.L., Wacker, L., Oleynik, S., Gersonde, R., and Haug, G.H.: Antarctic Zone
985 nutrient conditions during the last two glacial cycles, Paleoceanography, 30, 845–862,
986 https://doi.org/10.1002/2014PA002745, 2015.
987
988 Sun, X., and Matsumoto, K.: Effects of sea ice on atmospheric pCO2: A revised view and
989 implications for glacial and future climates. J. Geophys. Res., 115,
990 https://doi.org/10.1029/2009JG001023, 2010.
991
992 Toggweiler, J. R.: Variation of atmospheric CO2 by ventilation of the ocean's deepest
993 water, Paleoceanography, 14, 571–588, https://doi.org/10.1029/1999PA900033, 1999.
994
995 Warnock, J.P., and Scherer, R.P.: A revised method for determining the absolute abundance of
996 diatoms, J. Paleolimnol., 53, 157–163, https://doi.org/10.1007/s10933-014-9808-0, 2015.
997
998 Wilks, J. V., and Armand, L. K.: Diversity and taxonomic identification of Shionodiscus spp. in the
999 Australian sector of the Subantarctic Zone. Diatom Res., 32, 295–307,
1000 https://doi.org/10.1080/0269249X.2017.1365015, 2017.
1001
1002 Williams, M. J.: Voyage Report TAN1302, Mertz Polynya (Tech. Rep.) Wellington: National
1003 Institute of Water and Atmospheric Research (NIWA), 2013.
1004
1005 Williams, T.J., Martin, E.E., Sikes, E., Starr, A., Umling, N.E., & Glaubke, R.: Neodymium isotope
1006 evidence for coupled Southern Ocean circulation and Antarctic climate throughout the last
1007 118,000 years, Quaternary Sci. Rev., 260, 106915,
1008 https://doi.org/10.1016/j.quascirev.2021.106915, 2021.
1009
1010 Wilson, D.J., Piotrowski, A.M., Galy, A., and Banakar, V.K. (2015). Interhemispheric controls on
1011 deep ocean circulation and carbon chemistry during the last two glacial cycles,
1012 Paleoceanography, 30, 621–641, https://doi.org/10.1002/2014PA002707, 2015.
1013
1014 Wolff, E.W., Barbante, C., Becagli, S., Bigler, M., Boutron, C.F., Castellano, E., de Angelis, M.,
1015 Federer, U., Fischer, H., Fundel, F., Hansson, M., Hutterli, M., Jonsell, U., Karlin, T., Kaufmann,
1016 P., Lambert, F., Littot, G.C., Mulvaney, R., Röthlisberger, R., and Wegner, A.: Changes in
1017 environment over the last 800,000 years from chemical analysis of the EPICA Dome C ice

core, Quaternary Sci. Rev., 29, 285–295, https://doi.org/10.1016/j.quascirev.2009.06.013,

1019 2010.